

1 Single-cell virus sequencing of 2 influenza infections that trigger 3 innate immunity

4 Alistair B. Russell¹, Jacob R. Kowalsky¹, Jesse D. Bloom^{1,2,3*}

*For correspondence:
jbloom@fredhutch.org (JDB)

5 ¹Basic Sciences Division and Computational Biology Program, Fred Hutchinson Cancer
6 Research Center, Seattle, United States; ²Department of Genome Sciences, University of
7 Washington, Seattle, United States; ³Howard Hughes Medical Institute, Fred Hutchinson
8 Cancer Research Center, Seattle, United States

10 **Abstract** The outcome of viral infection is extremely heterogeneous, with infected cells only
11 sometimes activating innate immunity. Here we assess how the genetic variation inherent in viral
12 populations contributes to this heterogeneity. We do this by developing a new approach to
13 determine both the transcriptome and full-length sequences of all viral genes in single
14 influenza-infected cells. Infections that activate an innate-immune response in single cells are
15 associated with viral defects that include amino-acid mutations, internal deletions, and failure to
16 express key genes. However, immune activation remains stochastic in cells infected by virions with
17 these defects, and sometimes occurs even in cells infected by virions that express unmutated
18 copies of all genes. Our work shows that the genetic variation present in influenza virus
19 populations substantially contributes to but does not fully explain the heterogeneity in infection
20 outcome and immune activation in single infected cells.

22 Introduction

23 Infection with an acute virus such as influenza initiates a race between the virus and immune
24 system. As the virus spreads, some infected cells trigger innate immunity and begin producing
25 interferon (IFN). This IFN directs expression of anti-viral interferon-stimulated genes (ISGs) in the
26 infected cell and its neighbors via autocrine and paracrine signaling, as well as helping launch a
27 broader immune response (*Stetson and Medzhitov, 2006; Honda et al., 2006*). If innate immunity
28 is activated sufficiently rapidly, it can reduce viral replication and disease severity (*Solov'ev, 1969;*
29 *Treanor et al., 1987; Beilharz et al., 2007; Kugel et al., 2009; Steel et al., 2010*)—although excessive
30 immune responses later in infection can actually be associated with immunopathology and more
31 severe disease (*La Gruta et al., 2007; Iwasaki and Pillai, 2014*).

32 Unfortunately for the host, influenza infection only rarely triggers IFN production by infected
33 cells early in infection (*Kallfass et al., 2013; Killip et al., 2017*). This rareness of IFN induction is just
34 one form of the extreme cell-to-cell heterogeneity that characterizes infection: cells also vary widely
35 in their production of viral mRNA, proteins, and progeny virions (*Russell et al., 2018; Steuerman*
36 *et al., 2018; Sjaastad et al., 2018; Heldt et al., 2015*). Because viral growth and the IFN response
37 are both feed-forward processes, early cell-to-cell heterogeneity could have significant downstream
38 consequences for the race between virus and immune system—especially since natural human
39 infections are typically initiated by just a few virions entering a few cells (*McCrone et al., 2018; Xue*
40 *and Bloom, 2018; Varble et al., 2014*).

41 It is unclear why only some infected cells trigger innate-immune responses. Two possible
42 contributors are pure stochasticity and pre-existing variation in cellular state. For instance, only
43 some cells induce IFN even upon treatment with synthetic innate-immune ligands (*Shalek et al.,*
44 *2013, 2014; Wimmers et al., 2018*), and the frequency of IFN induction may depend on a cell's pre-
45 existing chromatin state (*Bhushal et al., 2017*). But for influenza, a third possible contributor also
46 looms large: viral genetic diversity. Because influenza has a high mutation rate, even if the *consensus*
47 sequence of a viral population is "wild-type," individual virions will often have defects (*Parvin et al.,*
48 *1986; Suárez et al., 1992; Suárez-López and Ortín, 1994; Bloom, 2014; Pauly et al., 2017*). Indeed,
49 many studies have identified mutations that increase IFN induction when engineered into a viral
50 population (*te Velthuis et al., 2018; Du et al., 2018; Killip et al., 2017; Pérez-Cidoncha et al., 2014*),
51 and viral stocks that are rich in internal deletions in the polymerase genes induce more IFN (*Baum*
52 *et al., 2010; Tapia et al., 2013; Boergeling et al., 2015; Dimmock and Easton, 2015*).

53 However, existing techniques are inadequate to determine how viral genetic diversity con-
54 tributes to cell-to-cell heterogeneity during infection. Flow cytometry and fluorescent reporters only
55 measure protein levels (*Brooke et al., 2013; Guo et al., 2017*), and current single-cell transcriptomic
56 techniques primarily measure abundance of transcripts and provide only fragmentary information
57 on their sequences (*Russell et al., 2018; Zanini et al., 2018a,b; Steuerman et al., 2018; Saikia et al.,*
58 *2018; O'Neal et al., 2018*). None of these techniques reliably reveal if the virion infecting a specific
59 cell has some idiosyncratic mutation, despite the fact that such mutations are common even if cells
60 are infected with a nominally "wild-type" stock of virus.

61 Here we develop a new approach to measure both the full transcriptome and sequences of all
62 viral genes in single influenza-infected cells. To do this, we first enrich for rare IFN+ cells, and then
63 perform both standard Illumina-based single-cell transcriptomics and full-length PacBio sequencing
64 of viral genes. We obtain transcriptomes and sequences of all expressed viral genes in 150 infected
65 cells, 40 of which express IFN. Even though we used a "wild-type" stock of virus, two-thirds of cells are
66 infected by virions that have a mutation or defect in gene expression. This viral diversity is a major
67 contributor to cell-to-cell heterogeneity, with cells infected by truly wild-type virions having a tighter
68 distribution of viral transcriptional burden. Viral defects are especially common in IFN+ cells, and
69 we identify at least four types of defects that cause increased IFN induction. However, viral genetic
70 variation does not fully explain the heterogeneity, as even wild-type virions sometimes induce IFN.
71 Therefore, viral diversity is an important but not exclusive cause of cell-to-cell heterogeneity during
72 influenza infection.

73 Results

74 A system to identify and enrich for rare IFN+ positive cells

75 A challenge in studying IFN induction by influenza virus is the rareness with which infection triggers
76 its expression. We previously performed single-cell transcriptomics on hundreds of influenza-
77 infected A549 human lung epithelial cells at early times (6 to 10 hours) post-infection (*Russell*
78 *et al., 2018*), and found that only 1 of 368 infected cells expressed detectable type I or type III IFN
79 (*Figure 1A*). Prior studies using reporters have found that IFN expression is also rare in influenza-
80 infected mice at 24 and even 48 hours post-infection (*Kallfass et al., 2013*), a conclusion supported
81 by our own re-analysis of the single-cell transcriptomics of influenza-infected mice by *Steuerman*
82 *et al. (2018)* (see *Figure 1–Figure Supplement 1*).

83 To efficiently identify and enrich rare IFN+ cells, we created A549 cells that carried IFN re-
84 porters consisting of a type I (*IFNB1*) or type III (*IFNL1*) promoter driving expression of a cell-surface
85 protein (LNGFR Δ C; *Bonini et al., 1997; Ruggieri et al., 1997*) followed by a fluorescent protein (*Fig-*
86 *ure 1B*). Cells that activate the IFN reporter can be enriched by magnetic-activated cell sorting
87 (MACS) or identified by flow cytometry. The reporters were efficiently activated by a strain of
88 Sendai virus (*Strahle et al., 2006*) that potently induces IFN (*Figure 1–Figure Supplement 2*), and
89 activation of the type I and type III IFN reporters was highly correlated in our cells (*Figure 1–Figure*

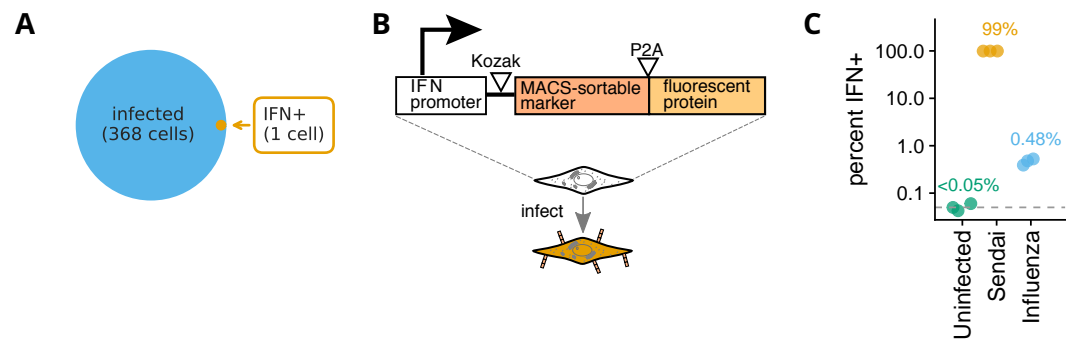


Figure 1. IFN expression is rare in influenza-infected cells. **(A)** Number of infected and IFN+ A549 cells in our prior single-cell transcriptomics (Russell et al., 2018). **(B)** An A549 reporter cell line to identify cells expressing IFN. The reporter consists of an IFN promoter that drives expression of a cell-surface protein amenable to MACS and a fluorescent protein. We created reporters with type I and type III IFN promoters (Figure 1–source data 1). The reporters were efficiently activated by an IFN-inducing strain of Sendai virus (Figure 1–Figure Supplement 2). **(C)** Frequency of IFN induction upon infection with the influenza virus stock used in the single-cell studies in this paper, as quantified using the reporter cell line (see Figure 1–Figure Supplement 4 for details). The plot also shows uninfected cells, and cells infected with saturating amounts of Sendai virus. The limit of detection of 0.05% is indicated with a dashed line, and numbers show the median of three measurements.

Figure 1–Figure supplement 1. Few cells express detectable IFN in influenza-infected mice.

Figure 1–Figure supplement 2. Validation of IFN reporter cell lines.

Figure 1–Figure supplement 3. Expression of type I and type III IFN is highly correlated in A549 cells.

Figure 1–Figure supplement 4. Full flow cytometry data for Figure 1C.

Figure 1–source data 1. Sequences of the reporters in Figure 1B are at https://github.com/jbloombalab/IFNsorted_flu_single_cell/tree/master/paper/figures/IFN_stochastic/IFN_reporter/plasmids.

90 **Supplement 3**; further validated by the single-cell transcriptomics below). Therefore, for the rest of
91 this paper, we use “IFN expression” to refer to combined expression of type I and III IFNs.

92 We generated a stock of “wild-type” A/WSN/1933 (H1N1) influenza (hereafter referred to as
93 “WSN”), and found that it activated the IFN reporter in ~0.5% of infected cells—a frequency roughly
94 comparable to that in our prior single-cell transcriptomics of influenza-infected cells (Figure 1A).

95 **Combined transcriptomics and virus-sequencing of single infected cells**

96 To determine if mutations or other features of the infecting virions contribute to the heterogeneous
97 outcome of infection, we developed the approach in Figure 2 to determine the entire transcriptome
98 and the full sequences of all viral genes in single cells. First, we generated a stock of virus that
99 consisted of a mix of wild-type WSN and a “synonymously barcoded” variant that contained two
100 engineered synonymous mutations near each termini of each gene (Figure 2–source data 1). These
101 viral barcodes allow us to identify co-infections from single-cell transcriptomic data (Russell et al.,
102 2018), and provide an important control for PCR artifacts during full-length sequencing of viral
103 transcripts (see below). We used this viral stock to infect A549 IFN reporter cells (Figure 2A) at a
104 dose that led to detectable viral transcription in about a quarter of cells. From 12 to 13 hours
105 post-infection, we used MACS to enrich cells that had activated the IFN reporter (Figure 2–Figure
106 Supplement 1). To ensure the presence of IFN- cells, we added back non-enriched cells to ~10% of
107 the total. We also added uninfected canine cells to ~5% of the total as a control for multipllets and
108 to estimate the background amount of viral mRNA detected in truly uninfected cells.

109 We processed the cells on a commercially available platform (Zheng et al., 2017) that isolates
110 cells in droplets and reverse transcribes polyadenylated mRNAs to append a unique cell barcode
111 to all cDNAs in each droplet, and a unique molecular identifier (UMI) to each cDNA molecule
112 (Figure 2B). Because influenza virus mRNAs are polyadenylated (Robertson et al., 1981), this process
113 appends cell barcodes to both cellular and viral mRNAs. Furthermore, because virtually the entire

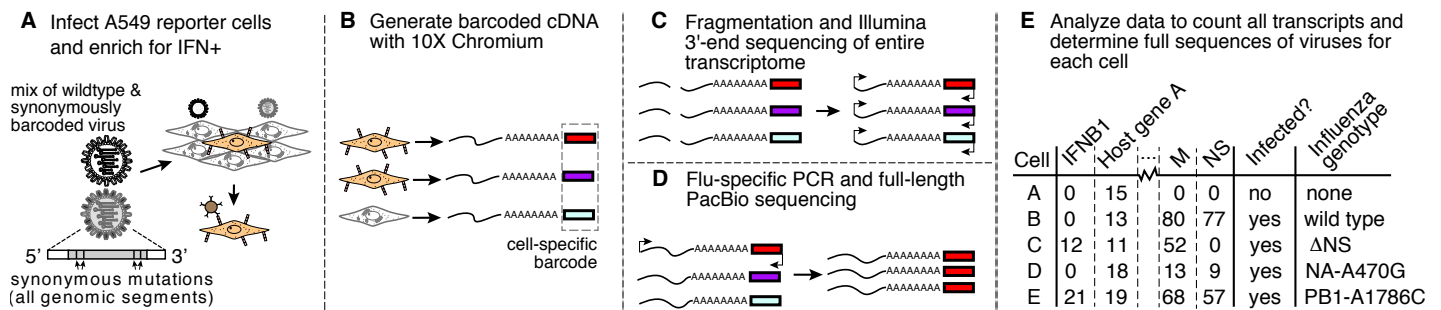


Figure 2. Approach for combined transcriptomic and viral sequencing of single influenza-infected cells that express IFN. **(A)** IFN reporter A549 cells are infected with a mix of wild-type and synonymously barcoded viruses. IFN+ cells are enriched by MACS (*Figure 2-Figure Supplement 1*), and pooled with non-enriched cells and uninfected canine cells that serve as an internal control for multiplets and mRNA leakage. **(B)** The mRNAs from individual cells are converted to cDNAs tagged with cell-specific barcodes. **(C)** Cellular transcriptomes are quantified using standard single-cell 3'-end Illumina sequencing, and **(D)** viral genes are enriched by influenza-specific PCR and fully sequenced by PacBio. **(E)** The result is a matrix giving the expression of each gene in each cell, as well as the full sequences of the viral genes in infected cells.

Figure 2-Figure supplement 1. MACS enrichment of IFN+ cells.

Figure 2-source data 1. Genbank files giving sequences of the wild-type and synonymously barcoded viruses are in https://github.com/jbloomlab/IFNsorted_flu_single_cell/blob/master/data/flu_sequences/flu-wsn.gb and https://github.com/jbloomlab/IFNsorted_flu_single_cell/blob/master/data/flu_sequences/flu-wsn-double-syn.gb.

114 influenza genome is transcribed, the cell-barcoded cDNA spans almost all 13,581 nucleotides in the
 115 segmented viral genome: the only portions not covered are one universally conserved nucleotide
 116 upstream of the transcription start site (*Koppstein et al., 2015*) and 17 to 22 highly conserved
 117 nucleotides downstream of the polyadenylation site (*Robertson et al., 1981*) in each of the eight
 118 viral gene segments.

119 We used a portion of the cell-barcoded cDNA for standard single-cell transcriptomics by Illumina
 120 3'-end sequencing (*Figure 2C*). But we also took a portion and enriched for full-length viral molecules
 121 by PCR (*Figure 2D*). We performed PacBio sequencing on these full-length viral cDNAs to generate
 122 high-accuracy circular consensus sequences (CCSs; *Travers et al., 2010*). These CCSs retain the cell
 123 barcodes, and with sufficient sequencing depth we obtain CCSs from multiple unique UMI-tagged
 124 cDNAs for each viral gene in each cell. Because most cells are infected by just one or two virions,
 125 we can build a consensus of CCSs for each viral gene in each cell to determine the sequence(s)
 126 of these virions. Combining this information with the 3'-end sequencing determines the entire
 127 transcriptome and the full sequences of the infecting virions in single cells (*Figure 2E*).

128 Transcriptomic analyses of single IFN+ and IFN- influenza-infected cells

129 We obtained transcriptomes for 1,614 human (A549) cells, and 50 of the uninfected canine cells that
 130 were spiked into the experiment as a control (*Figure 3A*). We also obtained 12 transcriptomes with a
 131 mix of human and canine transcripts; from the number of such mixed cell-type transcriptomes, we
 132 estimate (*Bloom, 2018*) that ~11% of the transcriptomes are derived from multiple cells. To remove
 133 some of these multiplets, we filtered transcriptomes with unusually high or low numbers of cellular
 134 transcripts (*Figure 3B*), retaining the 1,490 human cells that passed this filtering.

135 To identify infected cells, we examined the fraction of each transcriptome derived from virus (*Fig-*
 136 *ure 3B*). As expected, only a small fraction (~0.7%) of transcripts in the uninfected canine cells were
 137 from influenza; this low-level background is likely from lysed cells that release ambient viral mRNA
 138 that is captured in droplets during reverse-transcription. We tested whether each cell contained
 139 significantly more viral transcripts than expected under a Poisson model given this background
 140 fraction, and classified 290 human cells as definitively infected with influenza (*Figure 3B*). We classi-
 141 fied the other cells as uninfected, although it is possible that some were infected with virions that
 142 produced too little mRNA to be detected in our experiment. The distribution of the amount of viral
 143 mRNA across infected cells is shown in the inset in *Figure 3B*. As in our prior work (*Russell et al.,*

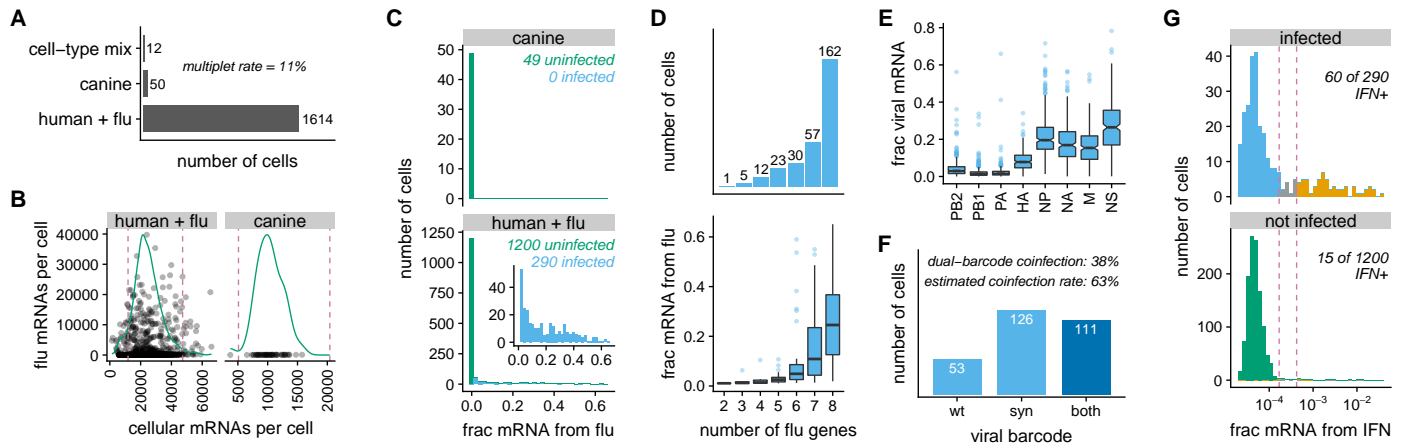


Figure 3. Single-cell transcriptomics of IFN-enriched influenza-infected cells. **(A)** Number of cells for which transcriptomes were obtained. From these numbers, we estimate (Bloom, 2018) that $\approx 11\%$ of the transcriptomes are actually multiplerts derived from multiple cells. **(B)** The number of cellular and viral mRNAs detected for each cell is plotted as a point. Green lines show the distribution of cellular mRNAs per cell. Cells outside the dashed magenta lines have unusually low or high amounts of cellular mRNA (likely low-quality emulsions or multiplerts), and are excluded from subsequent analyses. **(C)** Distribution across cells of the fraction of all mRNA derived from influenza. Cells called as infected are in blue, while other cells are in green. The inset shows the amount of viral mRNA in the human cells that are called as infected. **(D)** Number of influenza genes detected per infected cell, and the amount of viral mRNA in cells expressing each number of viral genes. The majority of cells express all eight gene segments, but a substantial minority fail to express at least one gene. **Figure 3–Figure Supplement 1** shows the frequency that each viral gene is detected. **(E)** Relative expression of viral genes among infected cells. **(F)** Number of cells infected with wild-type virus, synonymously barcoded virus, or both. From the cells infected with both viral barcodes, we estimate (Bloom, 2018) that 63% of infected cells are co-infected. **(G)** Fraction of cellular mRNA from IFN across cells, faceted by whether the cells are infected. Cells to the left of the first dashed magenta line are classified as IFN-, and cells to the right of the second line are classified as IFN+. A pseudocount is added to the number of IFN transcripts detected in each cell, which is why none of the fractions are zero. Many cells that do not express IFN still express ISGs (**Figure 3–Figure Supplement 3**).

Figure 3–Figure supplement 1. Fraction of infected cells that detectably express each influenza gene.

Figure 3–Figure supplement 2. Expression of type I and type III IFN is highly correlated in single cells in our experiment.

Figure 3–Figure supplement 3. Expression of ISGs in single infected and uninfected cells.

Figure 3–Figure supplement 4. Unsupervised t-SNE clustering shows that cell-to-cell variation in expression of influenza, IFN, and ISG transcripts substantially contributes to the structure of the data.

244 **2018**), the distribution is extremely heterogeneous: many infected cells have only a few percent of
 245 mRNA derived from virus, but viral mRNA comprises over half the transcriptome of a few cells.

246 We then called the presence or absence of each viral gene in each infected cell, again using
 247 a Poisson model parameterized by background fractions estimated from uninfected canine cells.
 248 We called presence / absence of genes rather than transcripts, since the two influenza genes that
 249 encode multiple transcripts (M1 / M2 from the M gene, and NS1 / NS2 from the NS gene) do so via
 250 alternative splicing that leaves both isoforms with the same termini, making them indistinguishable
 251 by 3'-end sequencing. **Figure 3D** (top panel) shows that most (162 of 290) infected cells express all
 252 eight genes, although a substantial minority fail to express one or more genes (see **Figure 3–Figure**
 253 **Supplement 1** for frequencies at which individual genes are present). This measured frequency of
 254 infected cells expressing all eight genes is slightly higher than in our own prior work (Russell et al.,
 255 **2018**) and studies by others (Brooke et al., 2013; Heldt et al., 2015; Dou et al., 2017), which have
 256 estimated that only 13% to 50% of infected cells express all genes.

257 The amount of viral mRNA tended to be lower in cells that failed to express viral genes (**Figure 3D**,
 258 bottom panel). However, viral burden remained highly variable even after conditioning on the
 259 number of viral genes: some cells that failed to express one or even two genes still derived $>50\%$ of
 260 their mRNA from virus, while other cells that expressed all genes had only a few percent of their
 261 mRNA from virus (**Figure 3D**, bottom panel). Consistent with our prior work (Russell et al., 2018),
 262 despite the wide variation in absolute expression of viral genes, their relative expression was fairly
 263 consistent (**Figure 3E**) and generally matched values from older bulk studies (Hatada et al., 1989).

164 By examining the synonymous viral barcodes near the 3' termini of transcripts, we determined
165 that 38% of cells were co-infected with wild-type and synonymously barcoded virions (**Figure 3F**;
166 cells called as co-infected if a binomial test rejected null hypothesis that $\geq 95\%$ of viral mRNA is from
167 one viral barcode variant). From **Figure 3F**, we estimate (**Bloom, 2018**) that 63% of infected cells are
168 co-infected, implying that 25% are co-infected with two virions with the same viral barcode (such
169 co-infections cannot be identified from transcriptomic data). Interestingly, this co-infection rate
170 is higher than expected from the relative numbers of infected and uninfected cells (**Figure 3C**) if
171 infection is Poisson. This discrepancy could arise if the MACS for IFN+ cells also enriches co-infected
172 cells, if infection is not truly Poisson, or if co-infection increases the likelihood that we identify a
173 cell as infected given the thresholds in **Figure 3C**. This moderately high rate of co-infection may
174 also explain why more cells in our experiment express all eight viral genes compared to some prior
175 studies, as a co-infecting virion can complement a missing viral gene (**Russell et al., 2018**).

176 We next examined expression of IFN and ISGs (**Figure 3G** and **Figure 3–Figure Supplement 3**).
177 Over 20% of infected cells were IFN+ given the heuristic thresholds in **Figure 3C**, indicating that
178 the MACS successfully enriched IFN+ cells far beyond their initial frequency of $\sim 0.5\%$ (**Figure 1C**)
179 among infected cells. Few ($\sim 1.3\%$) uninfected cells were IFN+; the few that were present might be
180 because the MACS enriched for rare cells that spontaneously activated IFN, or because some cells
181 that we classified as uninfected were actually infected at low levels. Many more cells expressed ISGs
182 than IFN itself: the ratio of ISG+ to IFN+ cells was 1.8 among infected cells, and 7 among uninfected
183 cells (**Figure 3–Figure Supplement 3A**). The IFN+ cells were a subset of the ISG+ cells: IFN+ cells
184 always expressed ISGs, but many ISG+ cells did not express IFN (**Figure 3–Figure Supplement 3B**).
185 These results are consistent with the established knowledge that IFN is expressed only in cells that
186 directly detect infection, but that ISGs are also expressed via paracrine signaling in cells that do not
187 themselves detect infection (**Stetson and Medzhitov, 2006; Honda et al., 2006**).

188 Finally, we qualitatively examined how expression of viral genes, IFN, and ISGs relate to the
189 overall structure of the high-dimensional transcriptomic data. **Figure 3–Figure Supplement 4** shows
190 unsupervised t-SNE clustering (**Maaten and Hinton, 2008**) of the cells. Cells expressing high levels
191 of viral genes, IFN, and ISGs cluster together—and most of the structure in the t-SNE plot that is not
192 associated with these genes involves uninfected and IFN- cells.

193 **Full genotypes of viruses infecting single IFN+ and IFN- cells**

194 We next used PacBio sequencing (**Figure 2D**) to determine the full sequences of the viral genes
195 expressed in single infected cells. Using PCR enrichment (see Methods), we obtained over 200,000
196 high-quality PacBio CCSs that mapped to an influenza gene and contained a cell barcode and UMI
197 (**Figure 4–Figure Supplement 1**). Crucially, the synonymous viral barcodes at both termini of each
198 gene enabled us to confirm that PCR strand exchange (**Figure 4–Figure Supplement 2**) was rare
199 (**Figure 4–Figure Supplement 1**), meaning that the vast majority of CCSs correctly link the sequence
200 of the viral transcript to cell barcodes and UMIs that identify the cell and molecule of origin.

201 We called a mutation in a viral gene if it was found in least two CCSs originating from different
202 mRNAs (unique UMIs) and at least 30% of all CCSs for that gene in that cell. For cells co-infected
203 with both viral barcode variants, we called mutations separately for each viral variant. This strategy
204 reliably identifies mutations in virions that initiate infection of cells infected with at most one virion
205 of each viral barcode variant ($\sim 75\%$ of infected cells), as well as high-abundance mutations in
206 cells co-infected with multiple virions of the same viral barcode. It will not identify mutations that
207 arise within a cell after the first few rounds of viral genome replication, since such mutations will
208 not reach 30% frequency in that cell. Therefore, analogous to somatic variant calling in tumor
209 sequencing (**Xu et al., 2014; Cibulskis et al., 2013**), there is a limit to our detection threshold: we
210 cannot identify mutations that occur on just a small fraction of transcripts in a cell.

211 We could call the sequences of all expressed viral genes in the majority of infected cells (**Figure 4–**
212 **Figure Supplement 3**). We were most effective at calling full viral genotypes in cells that expressed
213 high amounts of viral mRNA and were infected by only one viral barcode variant (**Figure 4–Figure**



Figure 4. Viral genotypes and infection outcomes in single cells. Arrows indicate presence of a viral gene from one (light blue) or both viral barcode variants (dark blue). Circles and boxes indicate mutations or indels as described in the legend, with circle areas and box heights proportional to the fraction of CCSs with that mutation. For dual-barcode infections, mutations / indels for the wild-type and synonymously barcoded viral variants are shown in the top and bottom half of the arrows, respectively. Green boxes at left show the percent of all mRNA in that cell derived from virus. Orange boxes show the percent of cellular mRNA derived from IFN, with orange box frames indicating cells classified as IFN+ in *Figure 3G*.

Figure 4–Figure supplement 1. Number of PacBio CCSs and PCR strand exchange rate.

Figure 4–Figure supplement 2. Strategy for detecting strand exchange during sequencing of full-length viral genes.

Figure 4–Figure supplement 3. Number of cells for which genotype(s) of infecting viruses were completely determined.

Figure 4–Figure supplement 4. Genotypes and infection outcomes plotted separately for IFN+ and IFN- cells.

Figure 4–source data 1. A text file giving the primers used to amplify the influenza cDNAs for PacBio sequencing is at https://github.com/jbloomb/IFNsorted_flu_single_cell/tree/master/paper/figures/WorkflowSchematic/PacBio_primer_list.txt

Figure 4–source data 2. A CSV file giving the genotypes is at https://github.com/jbloomb/IFNsorted_flu_single_cell/blob/master/paper/figures/single_cell_figures/genotypes.csv.

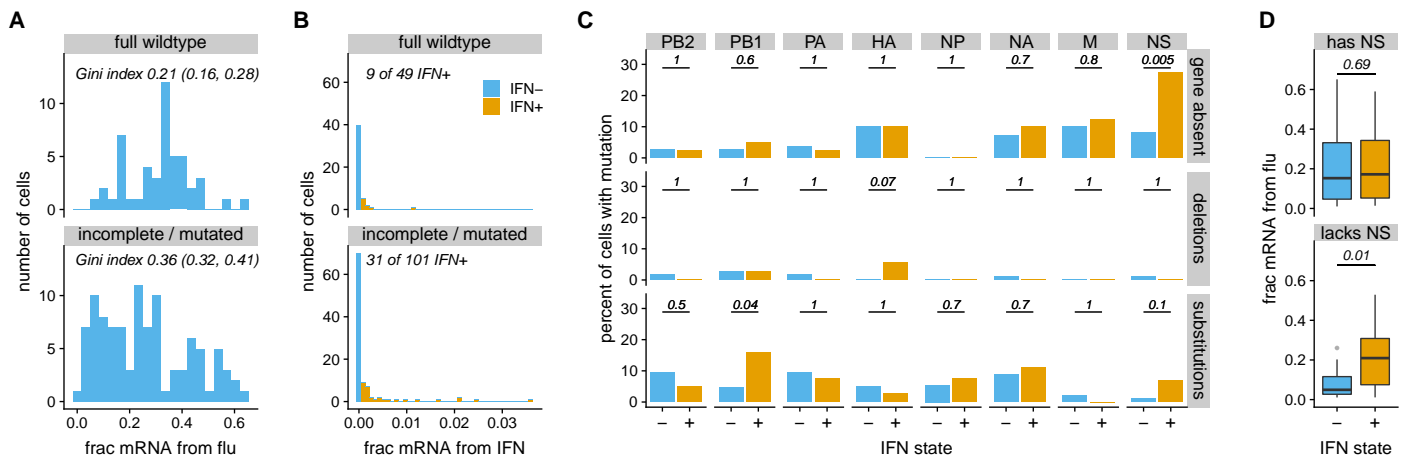


Figure 5. Viral features associated with heterogeneity in infection outcome among cells for which we sequenced all expressed viral genes. **(A)** Percent of all mRNA derived from virus, faceted by whether cells express unmutated copies of all eight genes. Cells infected by fully wild-type virus exhibit less heterogeneity in viral burden as quantified by the Gini index (95% confidence intervals are indicated). **(B)** IFN expression among cells expressing unmutated copies of all genes, and among cells with mutations or missing genes. **(C)** Specific viral defects associated with IFN induction. The top panel show the percent of IFN⁻ and IFN⁺ cells that fail to express each viral gene. The middle and bottom panels show the percent of IFN⁻ and IFN⁺ cells that have a deletion or amino-acid substitution in each gene, conditioned on the cell expressing that gene. Numbers give P-values (Fisher's exact test) for rejecting the null hypothesis that percents are equal among IFN⁻ and IFN⁺ cells. **Figure 5–Figure Supplement 1** and **Figure 5–Figure Supplement 2** show that the trends are similar if we include infected cells with incomplete viral sequence information, or categorize cells by ISG expression rather than IFN expression. **(D)** There is no association between IFN induction and the amount of viral mRNA in cells that express NS, but viral burden is associated with IFN induction among cells that lack NS. Throughout this figure, we only consider substitutions that are non-synonymous. Insertions are not shown as a mutation type as they are extremely rare (**Figure 4**).

Figure 5–Figure supplement 1. Analysis as in **Figure 5C** but including infected cells with incomplete viral sequence information.

Figure 5–Figure supplement 2. Association of viral genetic variation and ISG expression.

Figure 5–source data 1. A CSV file giving the viral mutations and related information in **Figure 5** is at https://github.com/jbloombloom/IFNsorted_flu_single_cell/blob/master/paper/figures/single_cell_figures/mutations.csv.

214 **Supplement 3**). But we also called full genotypes for many cells that had low viral burden or were
215 co-infected by both viral barcode variants.

216 The 150 cells for which we called the full viral genotypes are shown in **Figure 4**. Simple visual
217 inspection of this figure reveals a wealth of information. For instance, the cell with the highest
218 viral burden (*cell 1* in **Figure 4**, which has 65% of its mRNA from virus) was infected by a virion that
219 expressed wild-type copies all eight genes and did not induce detectable IFN. But 12 of the other
220 13 cells with at least 50% of their mRNA from virus were infected by virions that had a mutation
221 or failed to express at least one gene, and five of these cells expressed IFN. The two cells that
222 expressed the most IFN (*cell 13* and *cell 123*) both lacked the viral NS gene, and many other IFN⁺
223 cells had different defects such as large internal deletions (e.g., *cell 5* and *cell 89*) or amino-acid
224 mutations (e.g., *cell 9*, *cell 28*, and many others). However, expressing unmutated copies of all eight
225 genes did not guarantee a favorable outcome for the virus: for instance, the wild-type virion that
226 infected *cell 139* only managed to express viral mRNA to 6% of the total transcriptome, and the
227 wild-type virion that infected *cell 105* still induced IFN.

228 **Viral defects associated with infection outcome in single cells**

229 To systematically assess viral features associated with infection outcome, we divided the 150 cells in
230 **Figure 4** into those that expressed unmutated copies of all eight genes (disregarding synonymous
231 mutations) and those that did not. **Figure 5A** shows that the 49 cells infected by full wild-type
232 viruses had a significantly tighter distribution of the amount of viral mRNA per cell than the other
233 101 cells as quantified by the Gini index (*Gini, 1921*). Therefore, viral defects are a major contributor
234 to the heterogeneity in viral transcriptional burden among cells.

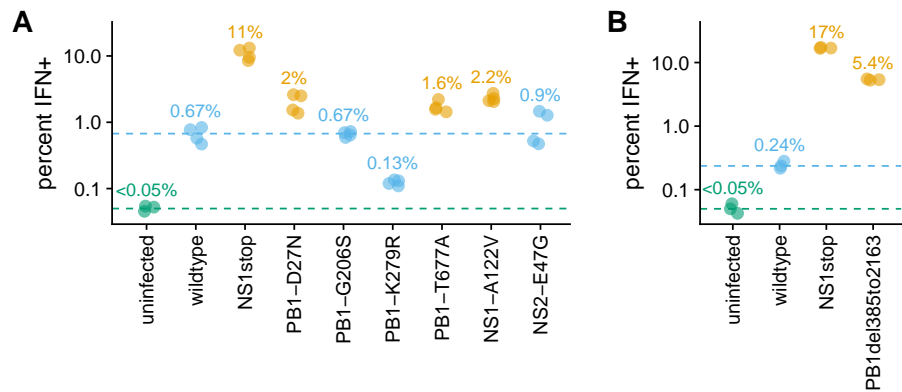


Figure 6. Validation that IFN induction is increased by some of the mutations identified in the single-cell virus sequencing of IFN+ cells. **(A)** Percent of cells that become IFN+ after infection with a bulk stock of the indicated viral mutant, as determined using a reporter cell line (see **Figure 6–Figure Supplement 1** for details). The numbers indicate the median of four measurements for each viral mutant. The limit of detection of 0.05% is indicated with a dashed green line, and the median value for wild type is indicated with a dashed blue line. Points are colored orange if the mutant virus stock induces IFN more frequently than the wild-type viral stock (one-sided t-test, $P < 0.01$), and blue otherwise. **(B)** Similar to the first panel, but validates the increased IFN induction for a large internal deletion in the PB1 gene. See **Figure 6–Figure Supplement 2** and **Figure 6–Figure Supplement 3** for more detailed experimental data. The experiments in the two panels were performed on different days, and so numerical values can be reliably compared within panels but not between panels.

Figure 6–Figure supplement 1. Flow cytometry data for **Figure 6A**.

Figure 6–Figure supplement 2. Flow cytometry data for **Figure 6B**.

Figure 6–Figure supplement 3. Validation of viral titer normalization for **Figure 6B**.

Figure 6–source data 1. Genbank plasmid maps for the mutant genes cloned into the pHW* bi-directional reverse genetics plasmid (*Hoffmann et al., 2000*) are at https://github.com/jbloomlab/IFNsorted_flu_single_cell/tree/master/paper/figures/FluVariantPlasmidMaps

235 Cells infected by incomplete or mutated virions also expressed IFN more frequently than cells
 236 infected by full wild-type virions (**Figure 5B**), although this difference was not statistically significant
 237 ($P = 0.12$, Fisher’s exact test). However, some specific viral defects were significantly associated with
 238 IFN induction: absence of NS and amino-acid mutations in PB1 were significantly enriched in IFN+
 239 cells, and amino-acid mutations in NS and deletions in HA were weakly enriched (**Figure 5C**). Due to
 240 the low number of cells and large number of hypotheses in **Figure 5C**, the only trend that remained
 241 significant at a false discovery rate of 10% was absence of NS.

242 One other interesting trend emerges from the single-cell data. There is no difference in the
 243 amount of viral mRNA between IFN+ and IFN- cells that express NS—but among cells that lack NS,
 244 the IFN+ ones have significantly more viral mRNA (**Figure 5D**).

245 **Validation that viral defects in single IFN+ cells often cause increased IFN induction**

246 To test if the viral defects identified in single IFN+ cells play a causal role in triggering IFN expression,
 247 we used reverse genetics to generate bulk stocks of viruses with some of these defects.

248 The viral defect most strongly associated with IFN induction was failure to express the NS gene
 249 (**Figure 4, Figure 5C**). Although it is sometimes possible to use complementing cells to generate
 250 influenza viruses lacking a specific gene (*Fujii et al., 2003; Marsh et al., 2007*), we were unable to
 251 generate viruses that lacked NS. The NS gene encodes two proteins (NS1 and NS2), the first of which
 252 is influenza’s primary innate-immune antagonist (*García-Sastre et al., 1998; Hale et al., 2008*). We
 253 therefore mimicked the effect of absence of NS by creating a mutant virus (which we will term
 254 “NS1stop”) that had multiple stop codons early in the NS1 coding sequence.

255 The single-cell data also showed that amino-acid substitutions in the PB1 and NS genes were
 256 enriched in IFN+ cells (**Figure 4, Figure 5C**), so we created mutant viruses with many of the amino-

257 acid substitutions found in these genes among IFN+ cells. Overall, we created six such point-mutant
258 viruses: PB1-D27N, PB1-G206S, PB1-K279R, PB1-T677A, NS1-A122V, and NS2-E47G.

259 Finally, prior work has suggested that virions carrying internal deletions in the polymerase
260 genes can induce higher levels of IFN (*Baum et al., 2010; Tapia et al., 2013; Boergeling et al., 2015;*
261 *Dimmock and Easton, 2015*). Although such deletions are not significantly enriched among IFN+
262 cells in our single-cell data (*Figure 5C*), there is an IFN+ cell that has a deletion in PB1 spanning
263 nucleotides 385 to 2163 (*cell 5 in Figure 4*). We therefore created a virus carrying this deletion, and
264 propagated it in cells constitutively expressing PB1 protein.

265 We tested the rate of IFN induction by each viral stock using the reporter cells. *Figure 6* shows
266 that five of the eight mutant viral stocks induced IFN more frequently than wild type. The strongest
267 IFN induction was by the NS1stop virus, but the PB1 internal deletion and three of the point-mutant
268 viruses (PB1-D27N, PB1-T677A, and NS1-A122V) also induced IFN significantly more frequently
269 than wild type. The other three point mutants (PB1-G206S, PB1-K279R, and NS2-E47G) did not
270 increase IFN induction—an unsurprising finding, since we also expect some mutations without an
271 IFN-enhancing effect to be found in IFN+ cells by chance. But overall, the results in *Figure 6* validate
272 that the viral defects in single IFN+ cells often cause increased IFN production.

273 Discussion

274 We have determined the full sequences of all viral genes expressed in single influenza-infected cells,
275 and examined how viral mutations and gene-expression defects associate with infection outcome
276 in each cell. Methodologically, our major advance is to measure the *genotypes* of viruses in addition
277 to the abundance of viral components (i.e., transcripts, proteins, or progeny virions) as has been
278 done by prior single-cell studies (*Russell et al., 2018; Zanini et al., 2018a,b; Steuerman et al., 2018;*
279 *Saikia et al., 2018; O’Neal et al., 2018; Zhu et al., 2009; Schulte and Andino, 2014; Akpinar et al.,*
280 *2016; Heldt et al., 2015; Brooke et al., 2013*). Our method builds on the observation by *Saikia*
281 *et al. (2018)* and *Zanini et al. (2018b)* that fragmentary viral genetic information can be obtained
282 by more standard single-cell transcriptomic techniques. To make this information complete, we
283 have coupled single-cell transcriptomics with long-read PacBio sequencing of viral genes, a strategy
284 analogous to that used by *Gupta et al. (2018)* to obtain full-length isoforms of some cellular genes
285 in single cells.

286 This viral genetic information turns out to be crucial for understanding infection outcome and
287 innate-immune induction. Despite the fact that we used a low-passage viral stock generated from
288 plasmids encoding a “wild-type” influenza genome, most infected cells do not express wild-type
289 copies of all viral genes. Although our study is certainly not the first to note that influenza has a
290 high mutation rate (*Parvin et al., 1986; Suárez et al., 1992; Suárez-López and Ortín, 1994; Bloom,*
291 *2014; Pauly et al., 2017*) and sometimes fails to express genes (*Brooke et al., 2013; Heldt et al.,*
292 *2015; Dou et al., 2017; Russell et al., 2018*), it is the first to directly observe the full spectrum of
293 these defects across single cells. Visual inspection of *Figure 4* shows how any experiment that does
294 not sequence viral genes in single cells is averaging across a vast number of hidden viral defects.

295 It turns out that these viral defects substantially contribute to the heterogeneity observed in
296 prior single-cell studies of influenza (*Russell et al., 2018; Steuerman et al., 2018; Heldt et al., 2015;*
297 *Sjaastad et al., 2018*), including helping determine if an infected triggers an IFN response. We
298 identified four types of viral defects in single IFN+ cells that we validated to increase IFN induction.
299 Two types of defects—absence of the NS gene and amino-acid mutation to the NS1 protein—
300 presumably impair NS1’s well-known ability to antagonize innate-immune pathways (*García-Sastre*
301 *et al., 1998; Hale et al., 2008*). The third type of defect, amino-acid mutations in the PB1 protein,
302 is consistent with recent work by *te Velhuis et al. (2018)* showing that mutations to the viral
303 polymerase affect generation of mini-viral RNAs that activate the innate-immune sensor RIG-I.
304 Finally, we found an internal deletion in the PB1 gene that enhances IFN induction, consistent with
305 a large body of prior work showing that such deletions are immunostimulatory (*Baum et al., 2010;*
306 *Tapia et al., 2013; Boergeling et al., 2015; Dimmock and Easton, 2015*). Given the extensive prior

307 work describing such deletions, it is perhaps surprising we did not identify more of them in our
308 single IFN+ cells. There may be several reasons: we used relatively pure viral stocks (*Xue et al.,*
309 **2016**) at modest MOI; our experiments preferentially captured cells with higher viral transcriptional
310 load; and most prior studies have used techniques that can detect large deletions but not subtle
311 point mutations. The relative importance of different types of viral defects for IFN induction likely
312 varies across infection conditions, viral strains, and cell types—so it remains an open question as to
313 which defects are most relevant for early immune detection of actual viral infections in humans.

314 But although viral variation is clearly important, it still only partially explains heterogeneity
315 among influenza-infected cells. We find substantial breadth in viral transcriptional burden and
316 occasional IFN induction even among cells infected with fully wild-type virions. Additionally, none
317 of the viral defects in IFN+ cells induce IFN deterministically in our validation experiments—and
318 the apparently most immunostimulatory defect (absence of NS) also occurs in multiple IFN- cells in
319 our single-cell dataset. Of course, our single-cell virus sequencing only calls mutations present in a
320 cell at relatively high frequency, and so could overlook low-frequency mutations that contribute to
321 IFN induction. However, we suspect that stochasticity or pre-existing cellular states also affect the
322 outcome of infection, since heterogeneity in IFN induction is present even among cells treated with
323 synthetic innate-immune ligands (*Shalek et al., 2013, 2014; Wimmers et al., 2018; Bhushal et al.,*
324 **2017**), as well as for other viruses (*O'Neal et al., 2018*).

325 Perhaps the most intriguing question is how the heterogeneity that we have described ulti-
326 mately affects the macroscopic outcome of infection. Natural human influenza infections are
327 established by just a handful of virions (*McCrone et al., 2018; Xue and Bloom, 2018; Varble et al.,*
328 **2014**) that then undergo exponential growth, and early IFN responses are amplified by paracrine
329 signaling (*Stetson and Medzhitov, 2006; Honda et al., 2006*). It is therefore plausible that genetic
330 variation in the founding viral population could have a large effect on downstream events. Extend-
331 ing our approaches to more complex systems could shed further light on how viral genetic variation
332 interacts with cell-to-cell heterogeneity to shape the race between virus and immune system.

333 **Methods and Materials**

334 **IFN reporter cell lines**

335 We created IFN reporter variants of the A549 human lung epithelial cell line (**Figure 1B**). The parental
336 A549 cell line used to create these reporters was obtained from ATCC (CCL-185), and was tested as
337 negative for mycoplasma contamination by the Fred Hutch Genomics Core and authenticated using
338 the ATCC STR profiling service. The cells were maintained in D10 media (DMEM supplemented with
339 10% heat-inactivated fetal bovine serum, 2 mM L-glutamine, 100 U of penicillin / ml, and 100 μ g of
340 streptomycin / ml) at 37°C and 5% carbon dioxide.

341 To create the type I interferon reporters, a 1kb promoter region upstream of the human
342 IFNB1 gene were cloned into the pHAGE2 lentiviral vector (**O'Connell et al., 2010**), with a NotI site
343 immediately downstream of the promoter serving as an artificial Kozak sequence. Downstream of
344 this NotI site, each of the following reporter constructs was cloned: mCherry, mNeonGreen, and
345 low-affinity nerve growth factor lacking the C-terminal signaling domain (LNGFR Δ C) (**Bonini et al.,**
346 **1997; Ruggieri et al., 1997**) linked to mNeonGreen by a P2A linker (**Kim et al., 2011**). The sequence
347 of the last of these constructs is provided in **Figure 1-source data 1**.

348 To create the type III interferon reporters, a 1.2kb region upstream of the human IL29 (IFNL1)
349 gene was cloned into the pHAGE2 vector, with the native Kozak sequence retained at the 3' end.
350 Downstream of this promoter we cloned LNGFR Δ C linked to ZsGreen via a P2A linker. The sequence
351 of this construct is provided in **Figure 1-source data 1**.

352 We used these constructs to generate lentiviral vectors and transduce of A549 cells in the
353 presence of 5 μ g polybrene. We then sorted single transduced cells and expanded them. A portion
354 of the expanded cells were tested for reporter activity by transfecting poly(I:C) (a potent agonist of
355 the RIG-I pathway), and we retained clones with strong activation. Importantly, the cells that we
356 retained for further use were not the same portion that were tested by poly(I:C) treatment, but
357 rather a separate split of the same population—this avoids any selection on the cells from transient
358 activation of IFN. For the dual type I / type III reporter used in **Figure 1–Figure Supplement 3**, a
359 single-cell clone of the type III reporter cell line was transduced with the type I reporter bearing
360 the mCherry fluorescent marker, and then isolated and propagated as a single cell clone for the
361 other cell lines. All reporter lines tested negative for mycoplasma contamination by the Fred Hutch
362 Genomics Core.

363 **Figure 1–Figure Supplement 2** shows validation of the reporter cell lines using infection with
364 saturating amounts of the Cantell strain of Sendai virus (obtained from Charles River Laboratories).
365 For detection of the cell-surface bound LNGFR Δ C, cells were stained with PE-conjugated anti-LNGFR
366 (CD271) antibody from Miltenyi Biotec.

367 **Viruses for single-cell experiments**

368 We performed the single-cell experiments using the A/WSN/1933 (H1N1) strain of influenza virus.
369 We used both the wild-type virus and a variant of the virus where synonymous mutations were
370 added within a few 100 nucleotides of each termini of each gene segment. We have used a similar
371 synonymous viral barcoding strategy in our prior single-cell work (**Russell et al., 2018**) as it allows us
372 to detect about half of co-infected cells based on the expression of both viral barcode variants. In
373 the current work, we extended this approach by placing synonymous barcodes near *both* termini of
374 the gene segments in order to quantify strand exchange during PacBio sequencing (**Figure 4–Figure**
375 **Supplement 2**). The sequences of all gene segments from the wild-type and synonymously barcoded
376 viral strains are in **Figure 2-source data 1**. These genes were cloned into the pHW2000 (**Hoffmann**
377 **et al., 2000**) reverse-genetics plasmid.

378 Both viral strains were generated by reverse genetics using the pHW18* series of bi-directional
379 plasmids (**Hoffmann et al., 2000**). We controlled the durations and MOI during viral passaging
380 since these factors can greatly affect the accumulation of defective viral particles (**Xue et al., 2016**).
381 The viruses were generated by reverse genetics in co-cultures of 293T and MDCK-SIAT1 cells in

382 influenza growth media (Opti-MEM supplemented with 0.01% heat-inactivated FBS, 0.3% BSA, 100 U
383 of penicillin/ml, 100 μ g of streptomycin/ml, and 100 μ g of calcium chloride/ml) and then propagated
384 in MDCK-SIAT1 cells in influenza growth media using the same basic procedures detailed in *Russell*
385 *et al. (2018)*. Specifically, after generation by reverse genetics, the wild-type variant was expanded
386 at an MOI of 0.001 for 72 hours twice in MDCK-SIAT1 cells, and the synonymously barcoded variant
387 was expanded once at an MOI of 0.01 for 60 hours. The MOIs for this passaging are based on titers
388 determined using TCID50 assays via the formula of *Reed and Muench (1938)* as implemented at
389 <https://github.com/jbloomlab/reedmuenchcalculator>.

390 **Flow cytometry analyses for HA expression**

391 For the single-cell experiments (which only examine the transcriptional results of a single cycle of
392 infection), we were most interested in the titer of viral particles that are transcriptionally active
393 for a single round of infection of A549 cells. We estimated titers of transcriptionally active virions
394 by staining for HA expression in virus-infected A549 cells. Specifically, we infected A549 cells (or
395 one of the A549 reporter cell line variants as indicated) in influenza growth medium, and at 13
396 to 14 hours post-infection, we trypsinized cells, re-suspended in phosphate-buffered saline (PBS)
397 supplemented with 2% heat-inactivated fetal bovine serum (FBS), and stained with 10 μ g/ml of
398 H17-L19, a mouse monoclonal antibody previously shown to bind to the HA from the A/WSN/1933
399 strain of virus (*Doud et al., 2017*). After washing in PBS supplemented with 2% FBS, the cells were
400 stained with a goat anti-mouse IgG antibody conjugated to APC, washed, fixed in 1% formaldehyde
401 in PBS, washed again, and then analyzed by flow cytometry to determine the fraction expressing
402 detectable HA protein.

403 **Single-cell transcriptomics of IFN-enriched infected cells using 10X Chromium**

404 The single-cell transcriptomics and virus sequencing was performed using the A549 cells with the
405 *IFNB1* LNGFR Δ C-P2A-mNeonGreen reporter. A schematic of the experiment is shown in *Figure 2*.

406 The wild-type and synonymously barcoded viruses were mixed with the goal of adding equal
407 numbers of transcriptionally active HA-expressing virions of each virus strain. The cells were then
408 infected with this mixture at a dose designed to infect about half the cells (*Figure 3C* suggests that
409 the actual rate of detectable infection was slightly lower). Infections were allowed to proceed for
410 12 hours. The cells were then trypsinized, the trypsin was quenched with D10 media, and cells
411 were resuspended in de-gassed PBS supplemented with 0.5% bovine serum albumin and 5 mM
412 EDTA. To enrich IFN+ cells, the cells were then incubated with anti-LNGFR MACSelect Microbeads
413 (Miltenyi Biotec) and twice passed over an MS magnetic column (Miltenyi Biotec), retaining the
414 bound (and presumably IFN-enriched) population each time. This MACS sorting is expected to give
415 approximately the enrichment for IFN+ cells shown in *Figure 2-Figure Supplement 1*. The original,
416 unsorted, population was then added back in to ~10% of the final cell fraction in order to ensure the
417 presence of interferon negative cells. At this point, uninfected canine (MDCK-SIAT1) cells were also
418 added to ~5% of the final cell fraction to enable quantification of the cell multiplet rate (*Figure 3A*)
419 and background viral mRNA in uninfected cells (*Figure 3C*). We began this entire process of cell
420 collection and enrichment at 12 hours post-infection, but the process (which was performed at
421 room temperature) took about an hour, and thus we consider the cells to have been analyzed at 13
422 hours post-infection. The final cell suspension was counted using a disposable hemocytometer
423 and loaded on the 10x Genomics Chromium instrument (*Zheng et al., 2017*), targeting capture of
424 ~1,500 cells.

425 This sample was then processed to create libraries for Illumina 3'-end sequencing according to
426 the 10X Genomics protocol using the Chromium Single Cell 3' Library and Gel Bead Kit v2 with one
427 important modification: rather than process all full-length cDNA through enzymatic fragmentation,
428 several nanograms were retained for targeted full-length viral cDNA sequencing as described below.
429 The single-cell transcriptomics library was sequenced on an Illumina HiSeq 2500, and the data
430 analyzed as described below.

431 **Enrichment and preparation of viral cDNA for PacBio sequencing**

432 We amplified virus-derived molecules from the small amount of cDNA retained from the 10X
433 Genomics protocol for PacBio sequencing of the full-length cDNA. All molecules in this cDNA
434 have at their 3' end the cell barcode and UMI plus the constant adaptor sequence that is added
435 during the 10X protocol (see *Figure 2* for simple schematic, or the detailed analysis notebook
436 at https://github.com/jbloomlab/IFNsorted_flu_single_cell/blob/master/pacbio_analysis.ipynb or
437 Supplementary file 1 for at detailed schematic). However, we only wanted to PacBio sequence cDNA
438 molecules derived from virus, since it would be prohibitively expensive to sequence all molecules.
439 We therefore needed to enrich for the viral molecules, a process made challenging by the need
440 to also retain the 10X adaptor / UMI / cell barcode at the 3' end (the primer at the 5' end can be
441 specific, but the one at the 3' end must bind the common 10X adaptor shared among all molecules).

442 We first performed a multiplex PCR reaction on 1 ng of the full-length 10X cDNA using a 3'
443 primer complementary to the common 10X adaptor, and a multiplex mix of eight 5' primers, one
444 specific for the mRNAs from each of the eight viral gene segments (although some viral segments
445 produce multiple splice forms, all mRNAs from a given segment share the same 5' end). The
446 sequences of these primers are in *Figure 4-source data 1*. A major concern during these PCRs
447 is strand exchange (see *Figure 4-Figure Supplement 2*) which would scramble the cell barcodes
448 and mutations on viral cDNAs. To reduce strand-exchange and hopefully obtain more even PCR
449 amplification across segments, we performed emulsion PCRs using the Micellula DNA Emulsion
450 Kit (Roboklon). Emulsion PCR involves encapsidating DNA template molecules in a reverse-phase
451 emulsion, with each template positive droplet serving as a microreactor. This process physically
452 separates disparate template molecules, preventing strand exchange and allowing each molecule
453 to be amplified to exhaustion of its droplet's reagents without competing with the broader pool
454 of PCR-amenable molecules (*Boers et al., 2015*). We performed the PCRs using Kapa HiFi Hotstart
455 ReadyMix, supplementing the reactions with additional BSA to a final concentration of 0.1 mg/ml
456 and using a volume 100 μ l. Both the common 3' primer and the multiplex mix of eight 5' primers
457 were added to a final concentration of 0.5 μ M. We performed 30 cycles of PCR, using an extension
458 time of 2 minutes 15 seconds at 67°C, and a melting temperature of 95°C. This melting temperature
459 is lower than the standard 98°C melting step suggested by the manufacturer for Kapa HiFi because
460 we wanted to avoid collapse of emulsion integrity at high temperature. We performed 30 cycles
461 in order to saturate the reagents in each emulsion—unlike for open PCR reactions, the physical
462 occlusion of amplified material in emulsion PCR reduces artifacts at high cycle numbers.

463 Because we were concerned that the multiplex PCR would still result in highly uneven am-
464 plification of different influenza cDNAs due to differences in their expression levels and lengths,
465 the product of this multiplex PCR was subjected to eight additional individual emulsion PCR re-
466 actions, each using only a single segment-specific 5' primer as well as the common 3' primer,
467 using 1 ng of material in each reaction. The material from these eight segment-specific PCRs
468 was then pooled with the goal of obtaining a equimolar ratio of segments, and sequenced
469 on one SMRT Cell in a PacBio RS II and one SMRT Cell of a PacBio Sequel. Detailed results
470 from the analysis of these first two sequencing runs is shown in the PacBio analysis notebook
471 at https://github.com/jbloomlab/IFNsorted_flu_single_cell/blob/master/pacbio_analysis.ipynb and
472 Supplementary file 1. These results showed that although the PCRs substantially enriched for
473 influenza molecules, the relative coverage of the different viral genes was still very uneven, with the
474 longer genes (especially the polymerase genes) severely under-sampled.

475 To try to improve coverage of the polymerase genes, we produced two new sequencing pools:
476 one consisting of the five shortest viral segments (HA, NP, NA, M, and NS) from the aforementioned
477 segment-specific emulsion PCRs, and the other consisting of the three longer polymerase segments
478 (PB2, PB1, and PA). The former was sequenced on one cell of a single SMRT Cell of a PacBio Sequel,
479 and the latter on two additional SMRT Cells of a PacBio Sequel. As is shown in the PacBio analysis
480 notebook at https://github.com/jbloomlab/IFNsorted_flu_single_cell/blob/master/pacbio_analysis.

481 [ipy nb](#) (see also Supplementary file 1), even with these new sequencing runs the coverage remained
482 relatively low for the polymerase genes—and most of the reads we did obtain were dominated by
483 shorter internally deleted variants of the polymerase genes, which arise commonly during influenza
484 replication (*Xue et al., 2016*) and are presumably preferentially amplified during PCR.

485 To obtain more reads for longer full-length polymerase variants, we therefore subjected 10 ng of
486 our amplified material for each polymerase segment to a bead selection using SPRIselect beads at a
487 volume ratio of 0.4 to select for larger molecules. This selection removes most low-molecular weight
488 DNA species including internally-deleted defective segments. Material from this selection was
489 then amplified using 16 (PB1) or 14 (PB2 and PA) cycles of a non-emulsion PCR using the standard
490 conditions recommended by the Kapa HiFi Hotstart ReadyMix (extension at 67°C for 2 minutes
491 15 seconds, and melting at 98°C). The use of relatively few PCR cycles was designed to prevent
492 the occurrence of the artifacts (including strand exchange) that occur in non-emulsion PCRs as the
493 reactions approach saturation. We pooled the products of these reactions from this size-selection
494 and sequenced on a SMRT Cell of a PacBio Sequel. As is shown in the PacBio analysis notebook
495 at https://github.com/jbloomlab/IFNsorted_flu_single_cell/blob/master/pacbio_analysis.ipynb (see
496 also Supplementary file 1), this sequencing yielded modestly more full-length polymerase variants,
497 but they were still heavily undersampled compared to other viral genes.

498 To further to improve recovery of full-length PB1, PB2, and PA, we therefore took an alternative
499 approach that allowed us to perform a specific PCR for full-length polymerase variants. Specifically,
500 we circularized the template molecules (including the full length of genes plus the cell barcode,
501 UMI, and 10X adaptor), and then used two segment-specific primers that annealed in apposition
502 near the center of each polymerase gene to linearize these circular molecules. Only molecules
503 that contain the middle of the polymerase genes (which are typically full-length) are linearized by
504 this process. In the downstream computational analysis, we can then determine the full sequence
505 of the gene as well as the cell barcode of the initial molecule from which the linearized molecule
506 is derived. Specifically, we first used 2.5 ng of our already-amplified segment-specific material
507 in a 10-cycle PCR to append circularization adapters (see *Figure 4–source data 1* for sequences),
508 and cleaned the resultant mixture using SPRIselect beads at a volume ratio of 0.4. We then
509 used 10 ng of this amplified material in a 20 μ l NEBuilder reaction using an extended reaction
510 time of 50 minutes in order to circularize the molecules. We next incubated these reactions for
511 1 hour at 37°C with exonuclease V and additional ATP to a final increase in concentration of 1
512 mM to digest all non-circularized molecules. The circularized and digested material was then
513 cleaned using SPRIselect beads at a volume ratio of 0.4. This material was then used as template
514 for three non-emulsion PCRs specific to PB2, PB1, or PA, using two segment-specific primers
515 that align to the central portion of each gene but in apposition to each another (see *Figure 4–*
516 *source data 1* for sequences). These linearization reactions used 20 (PB2) or 26 (PB1 and PA) PCR
517 cycles, and the resulting products were cleaned using SPRIselect beads at a volume ratio of 1.0.
518 This material was pooled to produce an equimolar mixture of full-length PB1, PA, and PB2 and
519 sequenced in an additional SMRT Cell of PacBio Sequel. As is shown in the PacBio analysis notebook
520 at https://github.com/jbloomlab/IFNsorted_flu_single_cell/blob/master/pacbio_analysis.ipynb (see
521 also Supplementary file 1), this process efficiently yielded many full-length polymerase variants.

522 The computational analyses of the full-length viral gene sequences described below used the
523 combination of the data from all of these reactions. The number of sequences obtained for each
524 gene after pooling the data from all reactions is shown in *Figure 4–Figure Supplement 1*, which
525 also indicates that the net rate of strand exchange is very low (see *Figure 4–Figure Supplement 2*
526 for an illustration of how this is determined). A more detailed breakdown of the coverage of
527 each gene and data showing a consistently low rate of strand exchange for all PacBio runs is
528 at https://github.com/jbloomlab/IFNsorted_flu_single_cell/blob/master/pacbio_analysis.ipynb (see
529 also Supplementary file 1). Importantly, the various PCR biases and enrichment schemes mean that
530 the coverage of molecules by the PacBio sequencing is not proportional to their original abundance
531 in the starting mRNA. However, as described in the computational analysis section below, the final

532 analyses use the cell barcodes and UMIs in conjunction with the standard 10X Illumina sequencing
533 to ensure that none of the conclusions are affected by the disproportionate amplification of some
534 molecules during the PacBio library preparation (for instance, duplicate UMIs are removed from the
535 PacBio data, and all conclusions about gene abundance or absence are based on the Illumina data).

536 **qPCR for viral genes and IFN**

537 We performed qPCR on reverse-transcribed mRNA for influenza HA (to quantify viral transcription),
538 IFNB1 (to quantify IFN induction), and L32 (a cellular housekeeping gene for normalization). For the
539 qPCR, we used the SYBR Green PCR Master Mix (Thermo Fisher) according to the manufacturer's
540 protocol using oligo-dT primers. The qPCR primers were: HA primer 1, 5'-GGCCCAACCACACATTCAAC-
541 3'; HA primer 2, 5'-GCTCATCACTGCTAGACGGG-3'; IFNB1 primer 1, 5'-AAACTCATGAGCAGTCTGCA-3'; IFNB1
542 primer 2, 5'-AGGAGATCTTCAGTTTCGGAGG-3'; L32 primer 1, 5'-AGCTCCCAAAAATAGACGCAC-3'; L32 primer 2,
543 5'-TTCATAGCAGTAGGCACAAAGG-3'.

544 For the qPCR in **Figure 6–Figure Supplement 3**, A549 cells were seeded at a density of 10^4
545 cells/well in a 96-well plate in D10 media 24 hours prior to infection, with four independent wells
546 seeded per experimental treatment. Immediately prior to infection D10 media was removed and
547 replaced with influenza growth media and infected with the indicated influenza strains at a MOI of
548 0.4 based on TCID50 in MDCK-SIAT1 cells. For the cells with cycloheximide added to block protein
549 expression (and hence secondary transcription), cycloheximide was added to a final concentration
550 of 50 $\mu\text{g/ml}$ (a concentration sufficient to block secondary transcription; *Killip et al., 2014*) at the
551 time of infection. After 8 hours, mRNA was harvested using the CellAmp Direct RNA Prep Kit for
552 RT-PCR, reverse-transcribed using an oligo-dT primer, and qPCR was performed as described above.

553 **Viruses and experiments for validation experiments**

554 In **Figure 6**, we tested the IFN inducing capacity of a variety of viral mutants identified in the single-
555 cell experiments. For point-mutant viruses, we created variants for all amino-acid substitutions
556 found in PB1 and NS among IFN+ cells that did not also lack NS. One of these mutants (amino-acid
557 substitution S704P in PB1) did not reach sufficient titers in a single attempt to generate it by reverse
558 genetics, and so was dropped from the experiment (note that we did not attempt replicates of the
559 reverse genetics for this mutant, and so are *not* confident in drawing strong conclusions about its
560 actual attenuation). This left six point-mutant viruses: four with point mutations in PB1, and two
561 with point mutations in NS. We also created a mutant virus that contained the internal deletion
562 in PB1 found in an IFN+ cell. In addition, we created a virus with an inactivated NS1 to mimic the
563 infections that failed to express NS (we were unable to use complementing cells to generate a viral
564 stock that completely lacked the NS segment). This NS1stop virus contained six nucleotide changes
565 resulting in the addition of five in-frame stop codons in NS1 starting 10 nucleotides downstream of
566 the 5' splice donor site, thereby disrupting NS1 while leaving NS2 (NEP) intact. All of these mutants
567 were cloned into the pHW2000 bi-directional reverse-genetics plasmid (*Hoffmann et al., 2000*) in
568 order to enable generation of viruses encoding the mutant genes. **Figure 6–source data 1** provides
569 the full sequences for all of these plasmids.

570 We generated the wild-type and point-mutant viruses for the validation experiments in **Figure 6A**
571 by reverse genetics using the pHW18* series of WSN reverse genetics plasmids (*Hoffmann et al.,*
572 **2000**), but substituting the appropriate mutant plasmid listed in **Figure 6–source data 1** for the
573 wild-type plasmid for that gene. To generate the viruses from these plasmids, we transfected an
574 equimolar mix of all eight plasmids into co-cultures of 293T and MDCK-SIAT1 cells seeded at a ratio
575 of 8:1. At 24 hours post-transfection, we changed media from D10 to influenza growth media. At 50
576 hours post-transfection (for the replicate 1 viruses in **Figure 6–Figure Supplement 1**) or 72 hours
577 (for the replicate 2 viruses in **Figure 6–Figure Supplement 1**), we harvested the virus-containing
578 supernatant, clarified this supernatant by centrifugation at $300\times g$ for 4 min, and stored aliquots
579 of the clarified viral supernatant at -80°C . We then thawed aliquots and titered by TCID50 on
580 MDCK-SIAT1 cells. For the infections in **Figure 6–Figure Supplement 1**, we wanted to use equivalent

581 particle counts, so we normalized all viruses to an equivalent hemagglutination titer on turkey
582 red blood cells (*Hirst, 1942*). Briefly, a solution of 10% v/v red blood cells (LAMPIRE Biological
583 Laboratories, Fisher Scientific catalogue number 50412942) was washed in PBS and diluted to a
584 final concentration of 0.5% v/v. Two-fold serial dilutions of virus were added to an equal volume
585 of diluted red blood cells, and titer was measured as the highest dilution of viral stock at which
586 complete hemagglutination of red blood cells was observed. We then performed infections of the
587 A549 reporter cell line at equivalent hemagglutination titer and analyzed the data as described in
588 **Figure 6–Figure Supplement 1**.

589 To generate the NS1stop mutant virus and the wild-type and PB1del385to2163 mutant viruses
590 in **Figure 6–Figure Supplement 2**, we used slightly different procedures. The wild-type virus was
591 generated by reverse genetics as described for the point-mutant viruses above, harvested at
592 48 hours post-transfection, and then passaged on MDCK-SIAT1 cells for 36 hours at an MOI of
593 0.05—conditions that we previously validated to lead to relatively little accumulation of defective
594 particles (*Russell et al., 2018*). The NS1stop virus was similarly generated, but was passaged for
595 48 rather than 36 hours, since it had slower growth kinetics and so needed a longer period of
596 time to reach high titers. The viruses with deletions in the PB1 segment could not be generated
597 in normal 293T and MDCK-SIAT1 cells, since they required the exogenous expression of the PB1
598 protein. Therefore, these viruses were generated in previously described 293T and MDCK-SIAT1 cells
599 that had been engineered to constitutively express PB1 (*Bloom et al., 2010*). These viruses were
600 harvested from transfections at 72 hours, and passaged twice in the MDCK-SIAT1 cells constitutively
601 expressing PB1 at a MOI of 0.001 for 72 hours and 0.01 for 48 hours. This passaging was necessary
602 as viral titers from transfections were too low to generate sufficient virus from a single passage.
603 The wild-type and NS1stop viruses were titered by TCID50 on MDCK-SIAT1 cells, and the PB1
604 deletion viruses were titered on the MDCK-SIAT1 cells constitutively expressing PB1. The infections
605 in **Figure 6–Figure Supplement 2** were performed at equivalent TCID50s as described in the legend
606 to that figure. That these equivalent TCID50s were also roughly equivalent in terms of particles
607 capable of undergoing primary transcription is shown in **Figure 6–Figure Supplement 3**.

608 **Computational analysis of single-cell transcriptomic and viral sequence data**

609 A computational pipeline that performs all steps in the data analysis is available at https://github.com/jbloomlab/IFNsorted_flu_single_cell (*Russell and Bloom, 2018*). This pipeline is orchestrated
610 by Snakemake (*Köster and Rahmann, 2012*), and begins with the raw sequencing data and ends by
611 generating the figures shown in this paper. The sequencing data and annotated cell-gene matrix
612 are available on the GEO repository under accession GSE120839 (<https://www.ncbi.nlm.nih.gov/geo/query/acc.cgi?acc=GSE120839>).

615 Briefly, the raw deep sequencing data from the Illumina 3'-end sequencing were processed
616 using the 10X Genomics software package *cellranger* (version 2.2.0). We built a multi-species
617 alignment reference consisting of a concatenation of the human and influenza virus transcriptomes
618 (the first “species”) and the canine transcriptome (the second “species”). The human transcriptome
619 was generated by filtering genome assembly GRCh38 for protein-coding genes defined in GTF file
620 GRCh38.87. The influenza virus transcriptome consisted of the mRNAs for the wild-type A/WSN/1933
621 virus strain in **Figure 2–source data 1** (the *cellranger* alignment is sufficiently permissive that
622 it aligns sequences from both the wild-type and synonymously barcoded viral variants to this
623 transcriptome). The canine transcriptome was generated by filtering genome assembly CanFam3.1
624 for protein-coding genes defined in GTF file CanFam3.1.87. The *cellranger* software was used to
625 align the Illumina 3'-end sequencing reads to this multi-species transcriptome, call human+influenza
626 and canine cells (**Figure 3A**), and generate a matrix giving the expression of each gene in each single
627 cell. We used a custom Python script to determine the number of influenza virus reads that could
628 be assigned to the wild-type or synonymously barcoded virus, and added this information to the
629 annotated the cell-gene matrix.

630 The PacBio sequences of the full-length viral genes were analyzed as follows. First, we used

631 version 3.1.0 of PacBio's `ccs` program (<https://github.com/PacificBiosciences/unanimity>) to build
632 circular consensus sequences (CCSs) from the subreads files, requiring at least 3 passes and a
633 minimum accuracy of 0.999. We further processed these CCSs using custom Python code and
634 the `minimap2` (Li, 2018) long-read aligner (version 2.11-r797). The Python code has been imple-
635 mented in the API of `dms_tools2` (Bloom, 2015, https://jbloomlab.github.io/dms_tools2/) package
636 (version 2.3.0). A Jupyter notebook that performs these analyses is at [https://github.com/jbloomlab/
637 IFNsorted_flu_single_cell/blob/master/pacbio_analysis.ipynb](https://github.com/jbloomlab/IFNsorted_flu_single_cell/blob/master/pacbio_analysis.ipynb), and is also provided in HTML form as
638 Supplementary file 1. We refer the reader to this notebook for a detailed description and extensive
639 plots showing the results at each step. Here is a brief summary: we filtered for CCSs that had the
640 expected 5' termini (from the influenza-specific primers) and 3' termini (corresponding to the 10X
641 adaptor), and for which we could identify the cell barcode, UMI, and polyA tail. We aligned the
642 cDNAs flanked by these termini to the influenza transcriptome, and performed a variety of quality
643 control steps. At this point, we examined whether cDNAs had the synonymous viral barcodes at
644 both ends or neither end as expected in the absence of strand exchange (**Figure 4–Figure Supple-
645 ment 2**), and reassuringly found that strand exchange was rare (**Figure 4–Figure Supplement 1**).
646 The small number of CCSs with identifiable strand exchange were filtered from further analysis.
647 We then further filtered for CCSs that contained valid cell barcodes as identified by the `cellranger`
648 pipeline, and kept just one CCS per UMI (preferentially retaining high-quality CCSs that aligned to
649 full-length cDNAs). We then removed from the CCSs the barcoding synonymous mutations that we
650 had engineered into one of the two viral variants. Finally, we used the CCSs to call the sequence of
651 the viral gene in each cell, calling mutations separately for each viral barcode variant. We called
652 mutations (insertions, deletions, and substitutions) in the viral gene sequences as follows:

- 653 1. Mutations with accuracies less than 0.999 (which constitute <0.5% of all mutations) were
654 ignored.
- 655 2. If all CCSs for a particular viral-barcode variant of a gene in a cell were wild-type, it was called
656 as wild type.
- 657 3. If any CCSs for a particular viral-barcode variant of gene in a cell had a mutation, then require
658 at least two CCSs to call the sequence.
- 659 4. If at least two and >30% of the CCSs had a specific mutation, then call that mutation as
660 present and note its frequency among the CCSs. The exception was single-nucleotide indels
661 in homopolymers, for which we required three CCSs to call a mutation (the reason is that the
662 main mode of PacBio sequencing errors is short indels in homopolymers).

663 The plots in [https://github.com/jbloomlab/IFNsorted_flu_single_cell/blob/master/pacbio_analysis.
664 ipynb](https://github.com/jbloomlab/IFNsorted_flu_single_cell/blob/master/pacbio_analysis.ipynb) or Supplementary file 1 indicate that these are reasonable mutation-calling criteria. We could
665 call the sequences of all expressed viral genes in about half of the infected cells (**Figure 4–Figure
666 Supplement 3**). The mutations called using this pipeline are shown in **Figure 4**, and **Figure 4–source
667 data 2** gives the number of CCSs supporting each mutation call. The called sequences of the viral
668 genes were added to the annotated cell-gene matrix.

669 Finally, we process the annotated cell-gene matrix in R to generate the plots shown in this
670 paper. This analysis utilized a variety of R and Bioconductor (Huber et al., 2015) packages, including
671 `Monocle` (Qiu et al., 2017; Trapnell et al., 2014) and `ggplot2`. A Jupyter notebook that performs
672 these analyses is at [https://github.com/jbloomlab/IFNsorted_flu_single_cell/blob/master/monocle_
673 analysis.ipynb](https://github.com/jbloomlab/IFNsorted_flu_single_cell/blob/master/monocle_analysis.ipynb), and is also provided in HTML form as Supplementary file 2. We refer the reader
674 to this notebook for a detailed description and a variety of additional plots not included in the
675 paper. Briefly, we first filtered cells that were extreme outliers in the amount of mRNA as shown
676 in **Figure 3B**. We used the uninfected canine cells to estimate the percentage of total mRNA in a
677 cell that would come from influenza purely due to background (e.g., from cell lysis) in the absence
678 of infection, and called as infected the human cells for which significantly more than this amount
679 of mRNA was derived from influenza under a Poisson model (**Figure 3C**). We next used a Poisson
680 model parameterized by the amount of expected background mRNA for each influenza gene to call

681 the presence or absence of each influenza gene in each infected cell (**Figure 3D** and **Figure 3–Figure**
682 **Supplement 1**). To identify cells that were co-infected with both viral barcodes (**Figure 3F**), we used
683 a binomial test to identify cells for which we could reject the null hypothesis that at least 95% of
684 viral mRNA was derived from the more common viral barcode. We called IFN+ and ISG+ cells using
685 the heuristic thresholds shown in **Figure 3G** and **Figure 3–Figure Supplement 3**, respectively. We
686 counted IFN mRNAs as any IFN- α , IFN- β , or IFN- λ transcripts. We counted ISG mRNAs as any of
687 CCL5, IFIT1, ISG15, or Mx1. The plot in **Figure 4** summarizes all of the genotypic information, and
688 was created in substantial part using `gggenes` (<https://github.com/wilkox/gggenes>).

689 Acknowledgments

690 We thank Cole Trapnell, Jason Underwood, Robert Bradley, Daniel Stetson, AJ Velthuis, and Katherine
691 Xue for helpful suggestions. We thank Andy Marty and the Fred Hutch Genomics Core for performing
692 the deep sequencing. This work was supported by the NIAID of the NIH under grant R01 AI127893
693 and a Burroughs Wellcome Fund Young Investigator in the Pathogenesis of Infectious Diseases
694 grant to JDB. ABR was supported by a postdoctoral fellowship from the Damon Runyon Cancer
695 Research Foundation. JRK was supported by a Washington Research Foundation Undergraduate
696 Research Fellowship and a Mary Gates undergraduate research scholarship from the University
697 of Washington. JDB is an Investigator of the Howard Hughes Medical Institute. The funders had
698 no role in study design, data collection and interpretation, or the decision to submit the work for
699 publication.

700 Competing Interests

701 The authors declare that no competing interests exist.

References

- Akpinar F**, Timm A, Yin J. High-throughput single-cell kinetics of virus infections in the presence of defective interfering particles. *Journal of Virology*. 2016; 90(3):1599–1612.
- Baum A**, Sachidanandam R, García-Sastre A. Preference of RIG-I for short viral RNA molecules in infected cells revealed by next-generation sequencing. *Proceedings of the National Academy of Sciences*. 2010; 107(37):16303–16308.
- Beilharz MW**, Cummins JM, Bennett AL. Protection from lethal influenza virus challenge by oral type 1 interferon. *Biochemical and Biophysical Research Communications*. 2007; 355(3):740–744.
- Bhushal S**, Wolfsmüller M, Selvakumar T, Kemper L, Wirth D, Hornef M, Hauser H, Köster M. Cell Polarization and Epigenetic Status Shape the Heterogeneous Response to Type III Interferons in Intestinal Epithelial Cells. *Frontiers in Immunology*. 2017; 8:671–671.
- Bloom JD**, Gong LI, Baltimore D. Permissive Secondary Mutations Enable the Evolution of Influenza Oseltamivir Resistance. *Science*. 2010; 328(5983):1272–1275.
- Bloom JD**. An experimentally determined evolutionary model dramatically improves phylogenetic fit. *Molecular Biology and Evolution*. 2014; 31(8):1956–1978.
- Bloom JD**. Software for the analysis and visualization of deep mutational scanning data. *BMC Bioinformatics*. 2015; 16(1):168.
- Bloom JD**. Estimating the frequency of multiplets in single-cell RNA sequencing from cell-mixing experiments. *PeerJ*. 2018; 6:e5578.
- Boergeling Y**, Rozhdestvensky TS, Schmolke M, Resa-Infante P, Robeck T, Randau G, Wolff T, Gabriel G, Brosius J, Ludwig S. Evidence for a novel mechanism of influenza virus-induced type I interferon expression by a defective RNA-encoded protein. *PLoS Pathogens*. 2015; 11(5):e1004924.
- Boers SA**, Hays JP, Jansen R. Micelle PCR reduces chimera formation in 16S rRNA profiling of complex microbial DNA mixtures. *Nature Publishing Group*. 2015; p. 1–7.

- Boni MF**, Zhou Y, Taubenberger JK, Holmes EC. Homologous recombination is very rare or absent in human influenza A virus. *Journal of Virology*. 2008; 82(10):4807–4811.
- Bonini C**, Ferrari G, Verzeletti S, Servida P, Zappone E, Ruggieri L, Ponzoni M, Rossini S, Mavilio F, Traversari C, Bordignon C. HSV-TK gene transfer into donor lymphocytes for control of allogeneic graft-versus-leukemia. *Science*. 1997; 276(5319):1719–1724.
- Brooke CB**, Ince WL, Wrammert J, Ahmed R, Wilson PC, Bennink JR, Yewdell JW. Most influenza A virions fail to express at least one essential viral protein. *Journal of Virology*. 2013; 87:3155–3162.
- Cibulskis K**, Lawrence MS, Carter SL, Sivachenko A, Jaffe D, Sougnez C, Gabriel S, Meyerson M, Lander ES, Getz G. Sensitive detection of somatic point mutations in impure and heterogeneous cancer samples. *Nature Biotechnology*. 2013; 31(3):213–222.
- Dimmock NJ**, Easton AJ. Cloned defective interfering influenza RNA and a possible pan-specific treatment of respiratory virus diseases. *Viruses*. 2015; 7(7):3768–3788.
- Dou D**, Hernández-Neuta I, Wang H, Östbye H, Qian X, Thiele S, Resa-Infante P, Kouassi NM, Sender V, Hentrich K, Mellroth P, Henriques-Normark B, Gabriel G, Nilsson M, Daniels R. Analysis of IAV replication and co-infection dynamics by a versatile RNA viral genome labeling method. *Cell Reports*. 2017; 20(1):251–263.
- Doud MB**, Hensley SE, Bloom JD. Complete mapping of viral escape from neutralizing antibodies. *PLoS Pathogens*. 2017; 13(3):e1006271.
- Du Y**, Xin L, Shi Y, Zhang TH, Wu NC, Dai L, Gong D, Brar G, Shu S, Luo J, Reiley W, Tseng YW, Bai H, Wu TT, Wang J, Shu Y, Sun R. Genome-wide identification of interferon-sensitive mutations enables influenza vaccine design. *Science*. 2018; 359(6373):290–296.
- Fujii Y**, Goto H, Watanabe T, Yoshida T, Kawaoka Y. Selective incorporation of influenza virus RNA segments into virions. *Proceedings of the National Academy of Sciences*. 2003; 100(4):2002–2007.
- García-Sastre A**, Egorov A, Matassov D, Brandt S, Levy DE, Durbin JE, Palese P, Muster T. Influenza A virus lacking the NS1 gene replicates in interferon-deficient systems. *Virology*. 1998; 252(2):324–330.
- Gini C**. Measurement of inequality of incomes. *The Economic Journal*. 1921; 31(121):124–126.
- Guo F**, Li S, Caglar MU, Mao Z, Liu W, Woodman A, Arnold JJ, Wilke CO, Huang TJ, Cameron CE. Single-cell virology: on-chip investigation of viral infection dynamics. *Cell Reports*. 2017; 21(6):1692–1704.
- Gupta I**, Collier PG, Haase B, Mahfouz A, Joglekar A, Floyd T, Koopmans F, Barres B, Smit AB, Sloan S, et al. Single-cell isoform RNA sequencing (SciSOR-Seq) across thousands of cells reveals isoforms of cerebellar cell types. *bioRxiv*. 2018; DOI: 10.1101/364950.
- Hale BG**, Randall RE, Ortín J, Jackson D. The multifunctional NS1 protein of influenza A viruses. *Journal of General Virology*. 2008; 89(10):2359–2376.
- Hatada E**, Hasegawa M, Mukaigawa J, Shimizu K, Fukuda R. Control of influenza virus gene expression: quantitative analysis of each viral RNA species in infected cells. *The Journal of Biochemistry*. 1989; 105(4):537–546.
- Heldt FS**, Kupke SY, Dorl S, Reichl U, Frensing T. Single-cell analysis and stochastic modelling unveil large cell-to-cell variability in influenza A virus infection. *Nature Communications*. 2015; 6:8938.
- Hirst GK**. The quantitative determination of influenza virus and antibodies by means of red cell agglutination. *Journal of Experimental Medicine*. 1942; 75(1):49–64.
- Hoffmann E**, Neumann G, Kawaoka Y, Hobom G, Webster RG. A DNA transfection system for generation of influenza A virus from eight plasmids. *Proceedings of the National Academy of Sciences*. 2000; 97(11):6108–6113.
- Honda K**, Takaoka A, Taniguchi T. Type I interferon gene induction by the interferon regulatory factor family of transcription factors. *Immunity*. 2006; 25(3):349–360.
- Huber W**, Carey VJ, Gentleman R, Anders S, Carlson M, Carvalho BS, Bravo HC, Davis S, Gatto L, Girke T, Gottardo R, Hahne F, Hansen KD, Irizarry RA, Lawrence M, Love MI, MacDonald J, Obenchain V, Oles AK, Pages H, et al. Orchestrating high-throughput genomic analysis with Bioconductor. *Nature Methods*. 2015; 12(2):115.
- Iwasaki A**, Pillai PS. Innate immunity to influenza virus infection. *Nature Reviews Immunology*. 2014; 14(5):315.

- Kalfass C**, Lienenklaus S, Weiss S, Staeheli P. Visualizing the Beta Interferon Response in Mice during Infection with Influenza A Viruses Expressing or Lacking Nonstructural Protein 1. *Journal of Virology*. 2013; 87(12):6925–6930.
- Killip MJ**, Smith M, Jackson D, Randall RE. Activation of the Interferon Induction Cascade by Influenza A Viruses Requires Viral RNA Synthesis and Nuclear Export. *Journal of Virology*. 2014; 88(8):3942–3952.
- Killip MJ**, Jackson D, Pérez-Cidoncha M, Fodor E, Randall RE. Single-cell studies of IFN- β promoter activation by wild-type and NS1-defective influenza A viruses. *Journal of General Virology*. 2017; 98(3):357–363.
- Kim JH**, Lee SR, Li LH, Park HJ, Park JH, Lee KY, Kim MK, Shin BA, Choi SY. High cleavage efficiency of a 2A peptide derived from porcine teschovirus-1 in human cell lines, zebrafish and mice. *PLoS One*. 2011; 6(4):e18556.
- Koppstein D**, Ashour J, Bartel DP. Sequencing the cap-snatching repertoire of H1N1 influenza provides insight into the mechanism of viral transcription initiation. *Nucleic Acids Research*. 2015; 43(10):5052–5064.
- Köster J**, Rahmann S. Snakemake—a scalable bioinformatics workflow engine. *Bioinformatics*. 2012; 28(19):2520–2522.
- Kugel D**, Kochs G, Obojes K, Roth J, Kobinger GP, Kobasa D, Haller O, Staeheli P, Von Messling V. Intranasal administration of alpha interferon reduces seasonal influenza A virus morbidity in ferrets. *Journal of Virology*. 2009; 83(8):3843–3851.
- La Gruta NL**, Kedzierska K, Stambas J, Doherty PC. A question of self-preservation: immunopathology in influenza virus infection. *Immunology and Cell Biology*. 2007; 85(2):85–92.
- Li H**. Minimap2: pairwise alignment for nucleotide sequences. *Bioinformatics*. 2018; 1:7.
- Maaten Lvd**, Hinton G. Visualizing data using t-SNE. *Journal of Machine Learning Research*. 2008; 9(Nov):2579–2605.
- Marsh GA**, Hatami R, Palese P. Specific residues of the influenza A virus hemagglutinin viral RNA are important for efficient packaging into budding virions. *Journal of Virology*. 2007; 81(18):9727–9736.
- McCrone JT**, Woods RJ, Martin ET, Malosh RE, Monto AS, Lauring AS. Stochastic processes constrain the within and between host evolution of influenza virus. *eLife*. 2018; 7:e35962.
- O’Connell RM**, Balazs AB, Rao DS, Kivork C, Yang L, Baltimore D. Lentiviral vector delivery of human interleukin-7 (hIL-7) to human immune system (HIS) mice expands T lymphocyte populations. *PLoS One*. 2010; 5(8):e12009.
- O’Neal JT**, Upadhyay AA, Wolabaugh A, Patel NB, Bosinger SE, Suthar MS. West Nile virus-inclusive single-cell RNA sequencing reveals heterogeneity in the type I interferon response within single cells. *bioRxiv*. 2018; DOI: 10.1101/434852.
- Parvin JD**, Moscona A, Pan W, Leider J, Palese P. Measurement of the mutation rates of animal viruses: influenza A virus and poliovirus type 1. *Journal of Virology*. 1986; 59(2):377–383.
- Pauly MD**, Procaro MC, Lauring AS. A novel twelve class fluctuation test reveals higher than expected mutation rates for influenza A viruses. *eLife*. 2017; 6:e26437.
- Pérez-Cidoncha M**, Killip M, Oliveros J, Asensio V, Fernández Y, Bengoechea J, Randall R, Ortín J. An unbiased genetic screen reveals the polygenic nature of the influenza virus anti-interferon response. *Journal of Virology*. 2014; 88(9):4632–4646.
- Qiu X**, Mao Q, Tang Y, Wang L, Chawla R, Pliner HA, Trapnell C. Reversed graph embedding resolves complex single-cell trajectories. *Nature Methods*. 2017; 14(10):979.
- Reed LJ**, Muench H. A simple method of estimating fifty per cent endpoints. *American Journal of Epidemiology*. 1938; 27(3):493–497.
- Robertson J**, Schubert M, Lazzarini R. Polyadenylation sites for influenza virus mRNA. *Journal of Virology*. 1981; 38(1):157–163.
- Ruggieri L**, Aiuti A, Salomoni M, Zappone E, Ferrari G, Bordignon C. Cell-surface marking of CD34+ -restricted phenotypes of human hematopoietic progenitor cells by retrovirus-mediated gene transfer. *Human Gene Therapy*. 1997; 8(13):1611–1623.

- Russell AB**, Bloom JD. Computer code for “Single-cell virus sequencing of influenza infections that trigger innate immunity”. GitHub. 2018; **Commit hash will be added when paper is final.** https://github.com/jbloombiolab/IFNsorted_flu_single_cell.
- Russell AB**, Trapnell C, Bloom JD. Extreme heterogeneity of influenza virus infection in single cells. *eLife*. 2018; 7:e32303.
- Saikia M**, Burnham P, Keshavjee SH, Wang MF, Heyang M, Moral-Lopez P, Hinchman MM, Danko CG, Parker JS, De Vlaminc I. Simultaneous multiplexed amplicon sequencing and transcriptome profiling in single cells. *bioRxiv*. 2018; DOI: 10.1101/328328.
- Schulte M**, Andino R. Single-cell analysis uncovers extensive biological noise in poliovirus replication. *Journal of Virology*. 2014; 88(11):6205–6212.
- Shalek AK**, Satija R, Adiconis X, Gertner RS, Gaublotte JT, Raychowdhury R, Schwartz S, Yosef N, Malboeuf C, Lu D, et al. Single-cell transcriptomics reveals bimodality in expression and splicing in immune cells. *Nature*. 2013; 498(7453):236–241.
- Shalek AK**, Satija R, Shuga J, Trombetta JJ, Gennert D, Lu D, Chen P, Gertner RS, Gaublotte JT, Yosef N, et al. Single cell RNA Seq reveals dynamic paracrine control of cellular variation. *Nature*. 2014; 510(7505):363.
- Sjaastad LE**, Fay EJ, Fiege JK, Macchietto MG, Stone IA, Markman MW, Shen S, Langlois RA. Distinct antiviral signatures revealed by the magnitude and round of influenza virus replication in vivo. *Proceedings of the National Academy of Sciences*. 2018; 115(38):9610–9615.
- Solov’ev V**. The results of controlled observations on the prophylaxis of influenza with interferon. *Bulletin of the World Health Organization*. 1969; 41(3-4-5):683.
- Steel J**, Staeheli P, Mubareka S, García-Sastre A, Palese P, Lowen AC. Transmission of pandemic H1N1 influenza virus and impact of prior exposure to seasonal strains or interferon treatment. *Journal of Virology*. 2010; 84(1):21–26.
- Stetson DB**, Medzhitov R. Type I interferons in host defense. *Immunity*. 2006; 25(3):373–381.
- Steuerman Y**, Cohen M, Peshes-Yaloz N, Valadarsky L, Cohn O, David E, Frishberg A, Mayo L, Bacharach E, Amit I, Gat-Viks I. Dissection of Influenza Infection In Vivo by Single-Cell RNA Sequencing. *Cell systems*. 2018; 6:679–691.e4.
- Strahle L**, Garcin D, Kolakofsky D. Sendai virus defective-interfering genomes and the activation of interferon-beta. *Virology*. 2006; 351(1):101–111.
- Suárez P**, Valcárcel J, Ortín J. Heterogeneity of the mutation rates of influenza A viruses: isolation of mutator mutants. *Journal of Virology*. 1992; 66(4):2491–2494.
- Suárez-López P**, Ortín J. An estimation of the nucleotide substitution rate at defined positions in the influenza virus haemagglutinin gene. *Journal of General Virology*. 1994; 75(2):389–393.
- Tapia K**, Kim Wk, Sun Y, Mercado-López X, Dunay E, Wise M, Adu M, López CB. Defective viral genomes arising in vivo provide critical danger signals for the triggering of lung antiviral immunity. *PLoS Pathogens*. 2013; 9(10):e1003703.
- Trapnell C**, Cacchiarelli D, Grimsby J, Pokharel P, Li S, Morse M, Lennon NJ, Livak KJ, Mikkelsen TS, Rinn JL. The dynamics and regulators of cell fate decisions are revealed by pseudotemporal ordering of single cells. *Nature Biotechnology*. 2014; 32(4):381.
- Travers KJ**, Chin CS, Rank DR, Eid JS, Turner SW. A flexible and efficient template format for circular consensus sequencing and SNP detection. *Nucleic Acids Research*. 2010; 38(15):e159.
- Treanor JJ**, Betts RF, Erb SM, Roth FK, Dolin R. Intranasally administered interferon as prophylaxis against experimentally induced influenza A virus infection in humans. *The Journal of Infectious Diseases*. 1987; 156(2):379–383.
- Varble A**, Albrecht RA, Backes S, Crumiller M, Bouvier NM, Sachs D, García-Sastre A, et al. Influenza A virus transmission bottlenecks are defined by infection route and recipient host. *Cell Host & Microbe*. 2014; 16(5):691–700.

- te Velthuis A**, Long J, Bauer DL, Fan R, Yen HL, Sharps J, Siegers J, Killip M, French H, Oliva-Martin MJ, Randall R, de Wit E, van Riel D, Poon L, Fodor E. Mini viral RNAs act as innate immune agonists during influenza virus infection. *Nature Microbiology*. 2018; DOI: 10.1038/s41564-018-0240-5.
- Wimmers F**, Subedi N, van Buuringen N, Heister D, Vивиé J, Beeren-Reinieren I, Woestenenk R, Dolstra H, Piruska A, Jacobs JF, et al. Single-cell analysis reveals that stochasticity and paracrine signaling control interferon-alpha production by plasmacytoid dendritic cells. *Nature Communications*. 2018; 9(1):3317.
- Xu H**, DiCarlo J, Satya RV, Peng Q, Wang Y. Comparison of somatic mutation calling methods in amplicon and whole exome sequence data. *BMC Genomics*. 2014; 15(1):244.
- Xue J**, Chambers BS, Hensley SE, López CB. Propagation and characterization of influenza virus stocks that lack high levels of defective viral genomes and hemagglutinin mutations. *Frontiers in microbiology*. 2016; 7:326.
- Xue KS**, Bloom JD. Reconciling disparate estimates of viral genetic diversity during human influenza infections. *bioRxiv*. 2018; DOI: 10.1101/364430.
- Zanini F**, Pu SY, Bekerman E, Einav S, Quake SR. Single-cell transcriptional dynamics of flavivirus infection. *eLife*. 2018; 7:e32942.
- Zanini F**, Robinson M, Croote D, Sahoo MK, Sanz AM, Ortiz-Lasso E, Albornoz LL, Suarez FR, Montoya JG, Pinsky BA, Quake S, Einav S. Virus-inclusive single cell RNA sequencing reveals molecular signature predictive of progression to severe dengue infection. *bioRxiv*. 2018; DOI: 10.1101/388181.
- Zheng GX**, Terry JM, Belgrader P, Ryvkin P, Bent ZW, Wilson R, Ziraldo SB, Wheeler TD, McDermott GP, Zhu J, et al. Massively parallel digital transcriptional profiling of single cells. *Nature Communications*. 2017; 8:14049.
- Zhu Y**, Yongky A, Yin J. Growth of an RNA virus in single cells reveals a broad fitness distribution. *Virology*. 2009; 385(1):39–46.

Supplementary file 1. An HTML rendering of the Jupyter notebook that analyzes the PacBio data to call the viral sequences in infected cells is available at https://github.com/jbloomlab/IFNsorted_flu_single_cell/raw/master/paper/figures/pacbio_single_cell_figures/pacbio_analysis.html. This notebook contains detailed descriptions of each step and plots illustrating the results, and is the best way to understand this part of the analysis in detail. The actual Jupyter notebook rendered here is available at https://github.com/jbloomlab/IFNsorted_flu_single_cell/blob/master/pacbio_analysis.ipynb.

Supplementary file 2. An HTML rendering of the Jupyter notebook that analyzes the annotated cell-gene matrix to generate the figures in this paper is available at https://github.com/jbloomlab/IFNsorted_flu_single_cell/raw/master/paper/figures/single_cell_figures/monocle_analysis.html. This notebook contains detailed descriptions of each step and plots illustrating the results, and is the best way to understand this part of the analysis in detail. The actual Jupyter notebook rendered here is available at https://github.com/jbloomlab/IFNsorted_flu_single_cell/blob/master/monocle_analysis.ipynb.

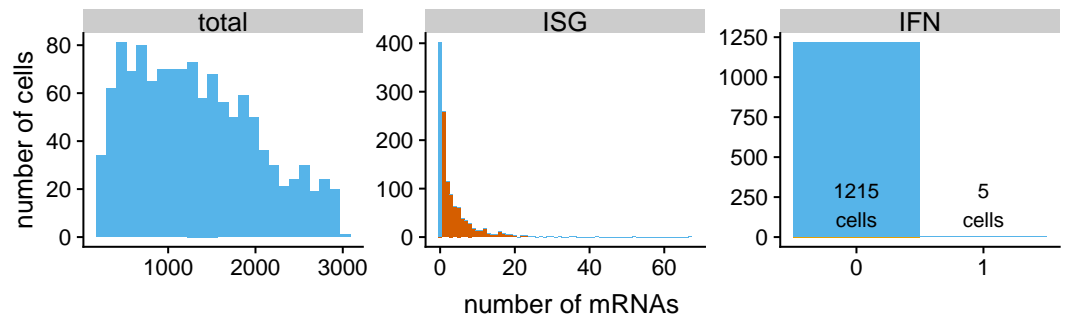


Figure 1-Figure supplement 1. A re-analysis of the data from *Steuerman et al. (2018)*'s single-cell transcriptomics of cells from influenza-infected mice shows that only 5 of 1220 virus-infected cells express *detectable* type I or type III IFN transcripts *in vivo*. Specifically, we downloaded the data from *Steuerman et al. (2018)* and identified influenza-infected cells using criteria similar to those described in *Steuerman et al. (2018)*. Here we show statistics for the cells from the influenza-infected wild-type C57BL/6J mice, which were collected at 48 hours (two replicates) or 72 hours (one replicate)—we do not show cells from the control mice. As shown in the left-most panel, the sequencing depth of *Steuerman et al. (2018)* was quite low, with only ~1,500 mRNA counts per cell on average (this is 10 to 15-fold lower than the sequencing depth in *Russell et al. (2018)* and the current study, respectively). An important caveat is that this low sequencing depth could lead to a simple failure to detect IFN transcripts in some cells. Nonetheless, there is detectable expression of key ISGs—which are induced by autocrine and paracrine signaling (*Stetson and Medzhitov, 2006; Honda et al., 2006*)—in the majority of infected cells (the middle panel shows the total counts of IFIT1, ISG15, CCL5, and Mx1). However, only 5 of 1220 cells express any detectable type I (IFN- α and IFN- β) or type III (IFN- λ) mRNAs, which are only induced by direct cellular detection of viral infection (*Stetson and Medzhitov, 2006; Honda et al., 2006*). The full code that performs the re-analysis shown in this figure is at https://github.com/jbloomlab/IFNsorted_flu_single_cell/tree/master/paper/figures/IFN_stochastic/SteuermanReanalysis/.

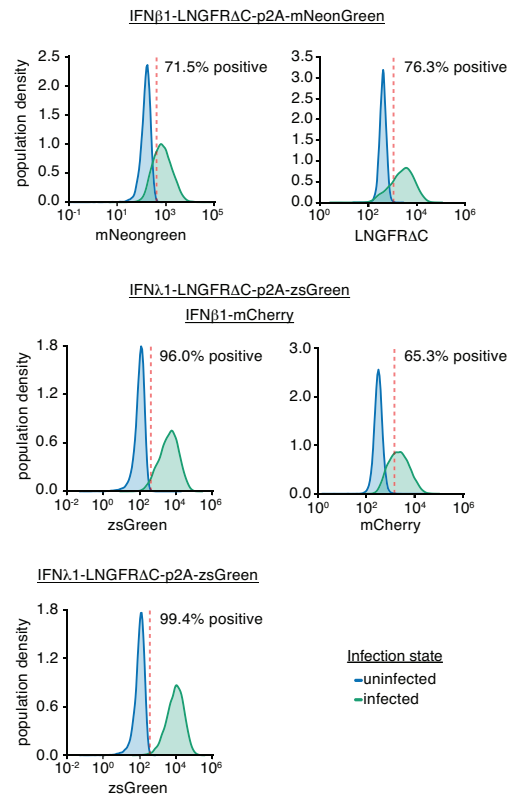


Figure 1-Figure supplement 2. To validate the IFN reporter cell lines, they were infected at high MOI with the Cantell strain of Sendai virus, which strongly activates IFN expression (*Strahle et al., 2006*). The name of each of reporter cell line is indicated at the top of each row of plots. At 13 hours post-infection, activation of the IFN reporter was then monitored by flow cytometry using the marker indicated at the bottom of each plot (either a fluorescent protein or antibody staining for the cell-surface LNGFR Δ C using a PE-conjugated anti-LNGFR antibody from Miltenyi Biotec). Sendai infection efficiently activated the IFN reporter in all cases, with the strongest signal from the IFN- λ reporter driving ZsGreen.

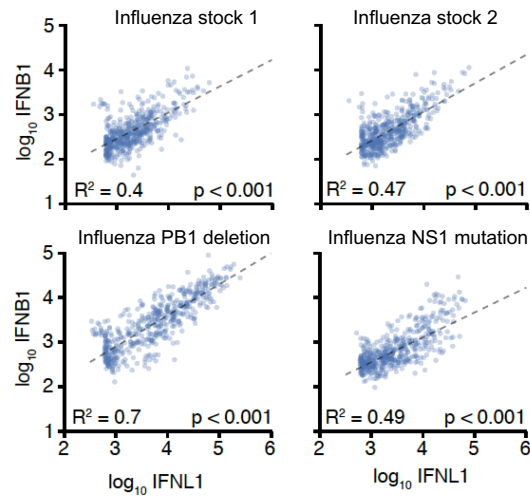


Figure 1-Figure supplement 3. An A549 cell line was generated by transduction with both the IFN- β and IFN- λ reporters driving expression of mCherry and ZsGreen, respectively. The cells were then infected with two different stocks of “wild-type” WSN influenza, or stocks with a deletion in PB1 or stop codons in NS1 (described later in the paper). After 13 hours, cells were analyzed by flow cytometry. Cells positive for either fluorescent reporter were further analyzed. As shown in the FACS plots, expression of the *IFNB1* and *IFNL1* reporters is highly correlated in all cases.

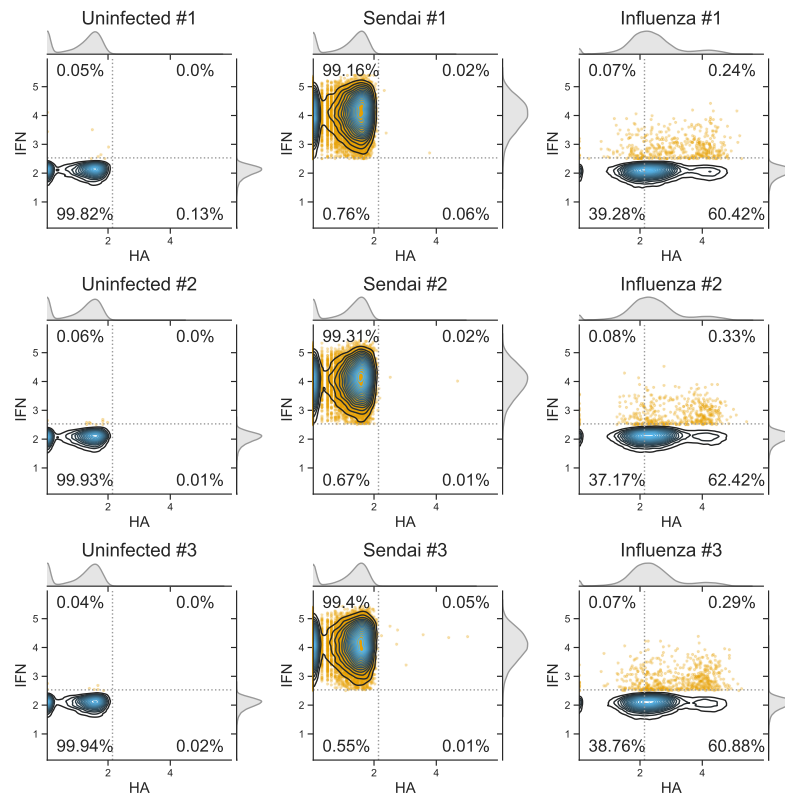


Figure 1-Figure supplement 4. Flow cytometry data for **Figure 1C**. The A549 cells with the *IFNL1* reporter driving LNGFR Δ C-ZsGreen were not infected, infected with saturating amounts of the Cantell strain of Sendai virus (Strahle et al., 2006), or infected the same stock of influenza virus used in the single-cell experiment at a target MOI of 0.3. After 13 hours, the cells were stained for expression of HA protein and analyzed by FACS for HA and expression of the ZsGreen driven by the *IFNL1* reporter. Each condition was done in triplicate. The contour plots show the density of all cells, and all IFN+ cells are also indicated by orange dots. Cells were classified as HA+ or IFN+ based on gates set to put 0.05% of the uninfected cells in these populations. For the influenza-infected cells, the percentage IFN+ was calculated only among the HA+ cells (since these are the ones that are infected). For the uninfected and Sendai-virus infected, the percentage IFN+ was calculated among all cells, since these cells do not express HA.

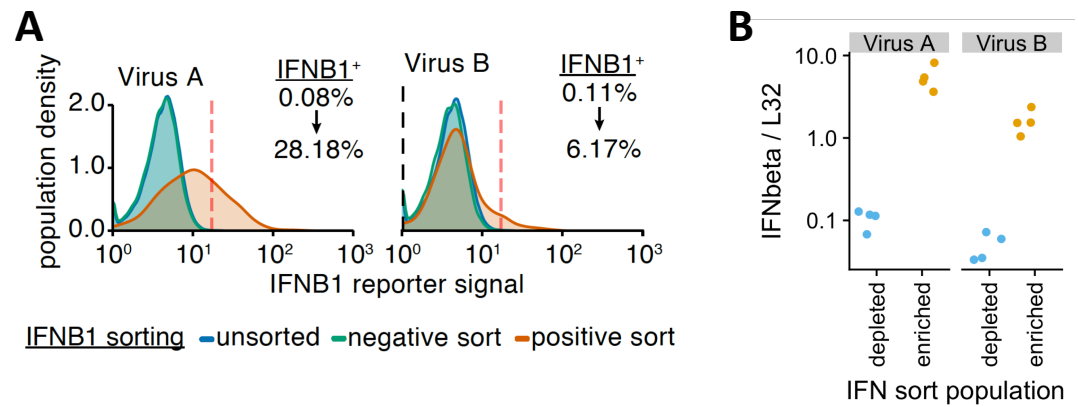


Figure 2-Figure supplement 1. Example MACS enrichments of IFN⁺ influenza-infected cells. A549 cells with the *IFNB1* LNGFR Δ C-mNeonGreen reporter were infected with wild-type WSN influenza (two different viral stocks) at a target MOI of 0.1 TCID₅₀ per cell. After infection had proceeded for 12 hours, the cells were twice magnetically sorted for LNGFR Δ C expression over magnetic columns as detailed in the methods for the single-cell sequencing experiment. **(A)** After sorting, the populations were analyzed by flow cytometry for IFN expression using the mNeonGreen fluorescent protein. The plots show the distribution of fluorescence in the original population, the flow-through from the first column, and the MACS-sorted positive population after two columns. As indicated by the percentages shown for the original and MACS-sorted population, this process led to substantial enrichment in IFN⁺ cells. We expect that the IFN sorting for the actual single-cell sequencing led to similar enrichment, although we could not directly quantify this as the sorted cells in that case were immediately used for the sequencing and so could not be analyzed by flow cytometry. **(B)** Analysis of expression of IFNB1 (relative to the housekeeping gene L32) by qPCR in the positive (IFN enriched) and negative (IFN depleted) populations from panel (A). The qPCR validates a roughly 50- to 100-fold enrichment in total IFNB1 expression. The qPCR was performed in quadruplicate (hence the four points for each sample).

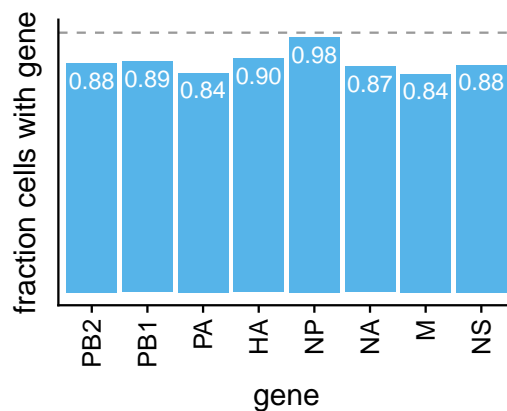


Figure 3-Figure supplement 1. The fraction of infected cells that are called as expressing each viral gene. The gray dashed line is at one (the fraction that would be observed if all viral genes are expressed in all infected cells). Each viral gene is detected in ~80-90% of the infected cells, roughly in line with prior estimates (*Brooke et al., 2013; Heldt et al., 2015; Dou et al., 2017; Russell et al., 2018*). The exception is NP, which is detected in virtually all infected cells. The much higher frequency of detecting NP could reflect a biological phenomenon, but we suspect it is more likely that cells lacking NP tend to have much lower viral gene expression overall and so are not reliably called as being infected in our experiments because the number of viral mRNAs is below the detection limit.

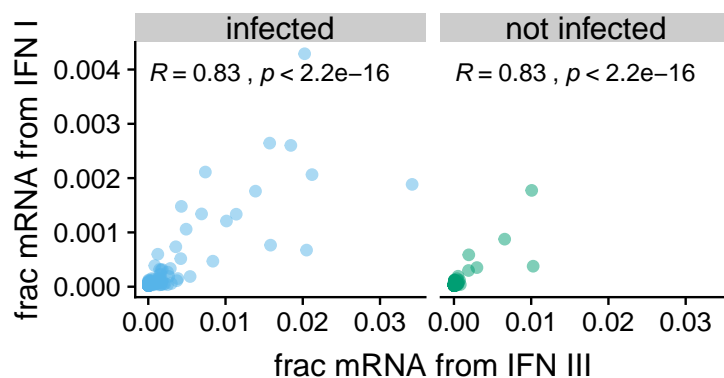


Figure 3-Figure supplement 2. The correlation between the fraction of cellular mRNA derived from type I and type III IFN in the A549 cells in our single-cell transcriptomics. Each point represents one cell. The plots are faceted by whether the cells are called as infected, and the Pearson correlation coefficient is shown. Because type I and type III IFN expression are highly correlated, for the remainder of the paper we group them together and refer to their combined expression as the level of IFN.

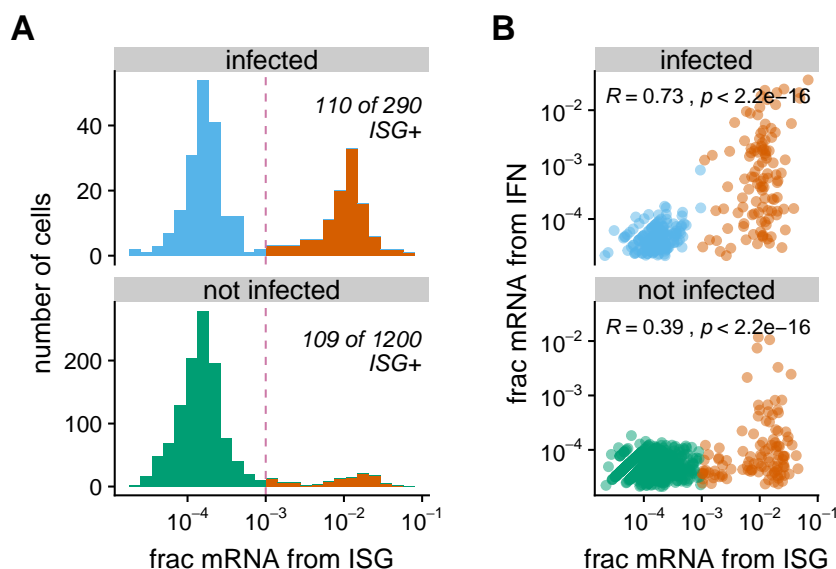


Figure 3-Figure supplement 3. For each cell, we quantified ISG expression as the total fraction of cellular mRNAs derived from four prototypical ISGs (IFIT1, ISG15, CCL5, and Mx1). **(A)** The histograms show the distribution of ISG expression taken across infected (top) and uninfected (bottom) cells. We heuristically classify as ISG+ cells with $> 10^{-3}$ of their cellular mRNA from ISGs, and color these cells red. Comparison to **Figure 3G** shows that substantially more cells are ISG+ than IFN+, both among infected and uninfected cells. This is probably because paracrine signaling can induce ISG expression in cells that are not themselves expressing IFN (*Stetson and Medzhitov, 2006; Honda et al., 2006*). **(B)** Correlation between the fraction of cellular mRNA derived from IFN and ISGs. Each point represents one cell, and the Pearson correlation coefficient is shown. IFN and ISG expression are more correlated for infected than uninfected cells, probably because in the latter the ISG expression is more often due to paracrine signaling that does not induce expression of IFN itself. Among both the infected and uninfected populations, there are many cells with high expression of ISGs and little expression of IFN, but no cells that express high levels of IFN without also substantially expressing ISGs.

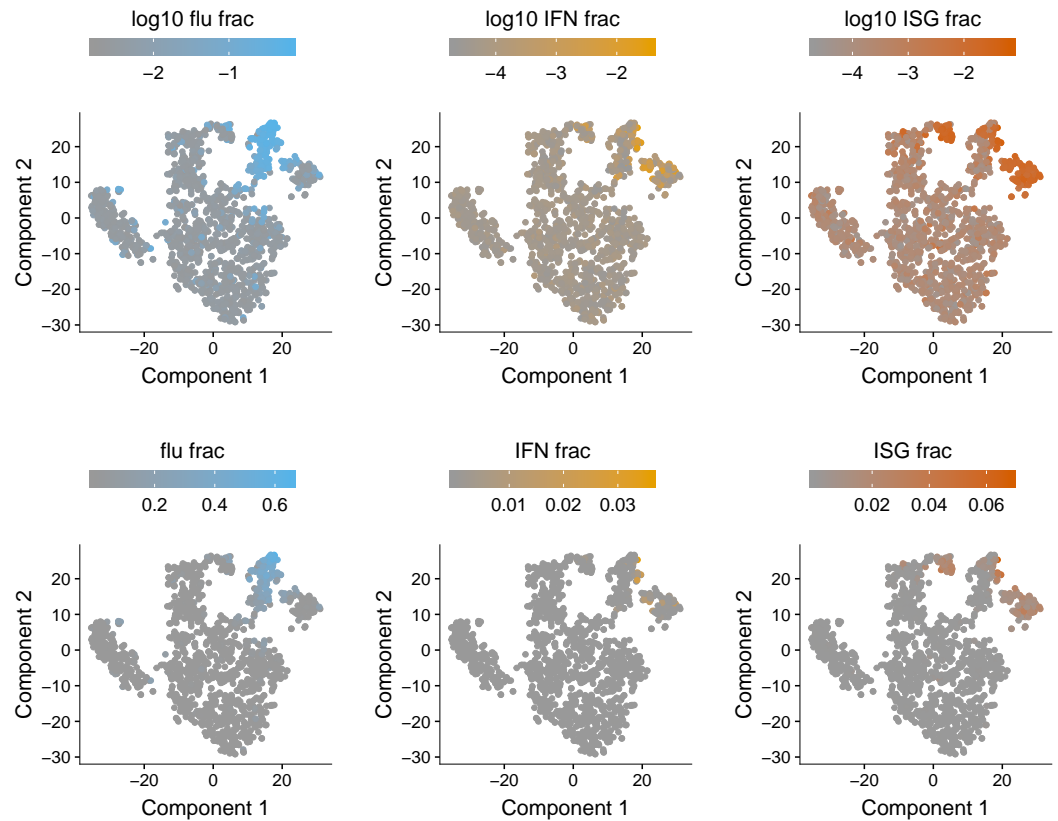


Figure 3-Figure supplement 4. To generate an unbiased representation of the factors that distinguished the transcriptomes of the cells in our experiments, we used unsupervised t-SNE clustering (*Maaten and Hinton, 2008*) as implemented in *MONOCLE* (*Qiu et al., 2017; Trapnell et al., 2014*) to generate a two-dimensional representation of the data. In the t-SNE plot, each point is a different cell, and cells with similar transcriptomes are closer together. Each panel shows the same t-SNE plot, but the cells are colored differently in each panel based on the amount of viral, IFN, or ISG mRNA, shown on a log (top) or linear (bottom) scale. As is clear from this plot, expression of influenza, IFN, and ISG genes contributes substantially to the structure of the data, since cells with high expression of these genes clearly group together.

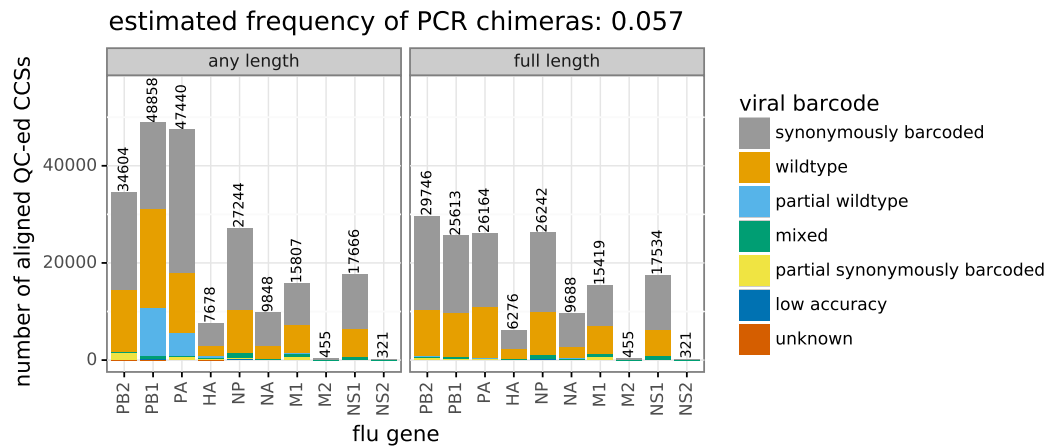


Figure 4–Figure supplement 1. The number of PacBio CCSs that passed quality-control steps and aligned to an influenza virus gene. Note that these sequences were obtained using several PacBio runs, most of which were intentionally loaded with different amounts of the various viral genes in order to increase coverage on genes that were needed in order to obtain the full sequences of virions infecting cells. (For exhaustive details, see the Jupyter notebook at https://github.com/jbloomlab/IFNsorted_flu_single_cell/blob/master/pacbio_analysis.ipynb and in Supplementary file 1.) Because of this unequal loading and the inherently different PCR amplification efficiencies of different viral genes, unlike the transcriptomic data in **Figure 3**, the numbers of CCSs for different genes should *not* be taken as an indicator of their abundance in the infected cells. Especially for the polymerase genes (PB2, PB1, and PA), many CCSs corresponded to genes with internal deletions, since these shorter forms of the genes were preferentially amplified during PCR. Therefore, the plot is faceted by the number of CCSs for any length of the gene, and for full-length genes. Note that the disproportionate sequencing of the shorter internally deleted genes should not greatly affect the genotype calling in **Figure 4** since UMIs were used to collapse duplicate sequences derived from the same cDNA, and cell barcodes were used to collapse duplicate sequences from the same cell. The bars in the plot are colored by whether the sequence is derived from the wild-type viral variant, the synonymously barcoded viral variant, or represents a mixed-barcode molecule (see **Figure 4–Figure Supplement 2** for more explanation). From the frequencies of these different forms, we estimate (*Bloom, 2018*) that 5.7% of molecules are chimeric due to PCR strand exchange. Note that about half of these PCR chimeras could be identified by the presence of mixed viral barcodes and removed from subsequent analyses, leaving ~3% un-identified chimeras. Note also that for some molecules (mostly polymerase genes with internal deletions) one of the barcode sites was deleted from the molecule and so the barcode identity could only be partially called. A negligible number of molecules have low-accuracy sequence or unexpected nucleotide identities at the sites of the viral barcodes.

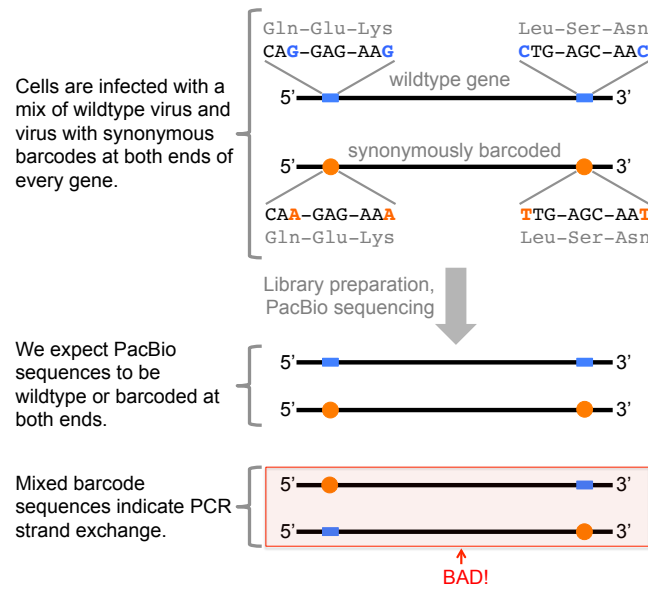


Figure 4–Figure supplement 2. The library preparation for PacBio sequencing of the cDNA for the full-length viral genes required many cycles of PCR. A major concern is that strand exchange during this PCR could scramble mutations and 10X cell barcodes / UMIs from different molecules. We can detect PCR strand exchange by leveraging the fact that our cells were infected with a mix of wild-type virus and virus carrying synonymous barcoding mutations near both termini of each gene. If there is no strand exchange, all molecules should either be wild-type or have the synonymous barcoding mutations at *both* termini. But strand exchange will create some molecules that have wild-type nucleotides at one termini and synonymous barcoding mutations at the other termini. **Figure 4–Figure Supplement 1** shows the frequencies with which these different types of molecules were observed during the PacBio sequencing. Note that since the rate of homologous recombination in influenza virus is negligible (*Boni et al., 2008*), such mixed-barcode molecules are *not* expected to be generated naturally during co-infection.

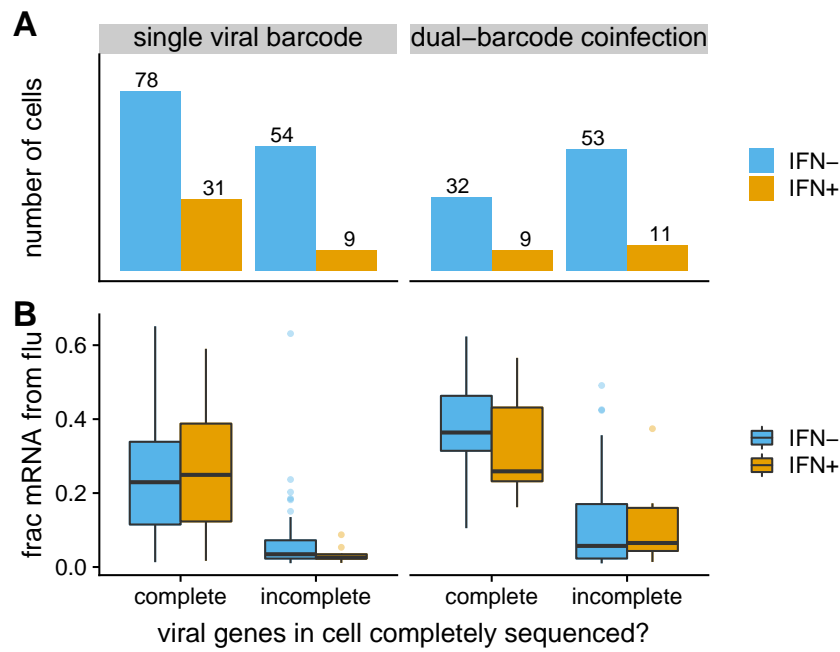


Figure 4-Figure supplement 3. Cells for which we could determine the full sequences of all genes expressed by the infecting virion(s). **(A)** We could call the complete genotypes of the infecting virion(s) for the majority of cells infected with just a single viral barcode variant, but only a minority of cells co-infected with both viral barcodes. **(B)** The cells for which we could call complete viral genotypes tended to have higher expression of viral mRNA than cells for which we could not call complete genotypes. Both facts makes sense. Cells with more viral mRNA are more likely to have their viral cDNA captured in the PacBio sequencing, which is only captures a small fraction of the total transcripts identified by the 3'-end sequencing transcriptomic sequencing. The lower calling rate for dual-barcode co-infections is probably because these co-infections have more viral genes that must be sequenced (potentially a copy of each viral gene from each viral variant), increasing the chances that one of these genes is missed by the PacBio sequencing. An important implication of this plot is that the cells for which we call complete viral genotypes are *not* a random subsampling of all infected cells in the experiment, but are rather enriched for cells that have high levels of viral mRNA and do not have dual-barcode viral infections. Note also that this plot is limited to the cells that were called as infected (**Figure 3C**) and could clearly be classified as IFN- or IFN+ (**Figure 3G**).

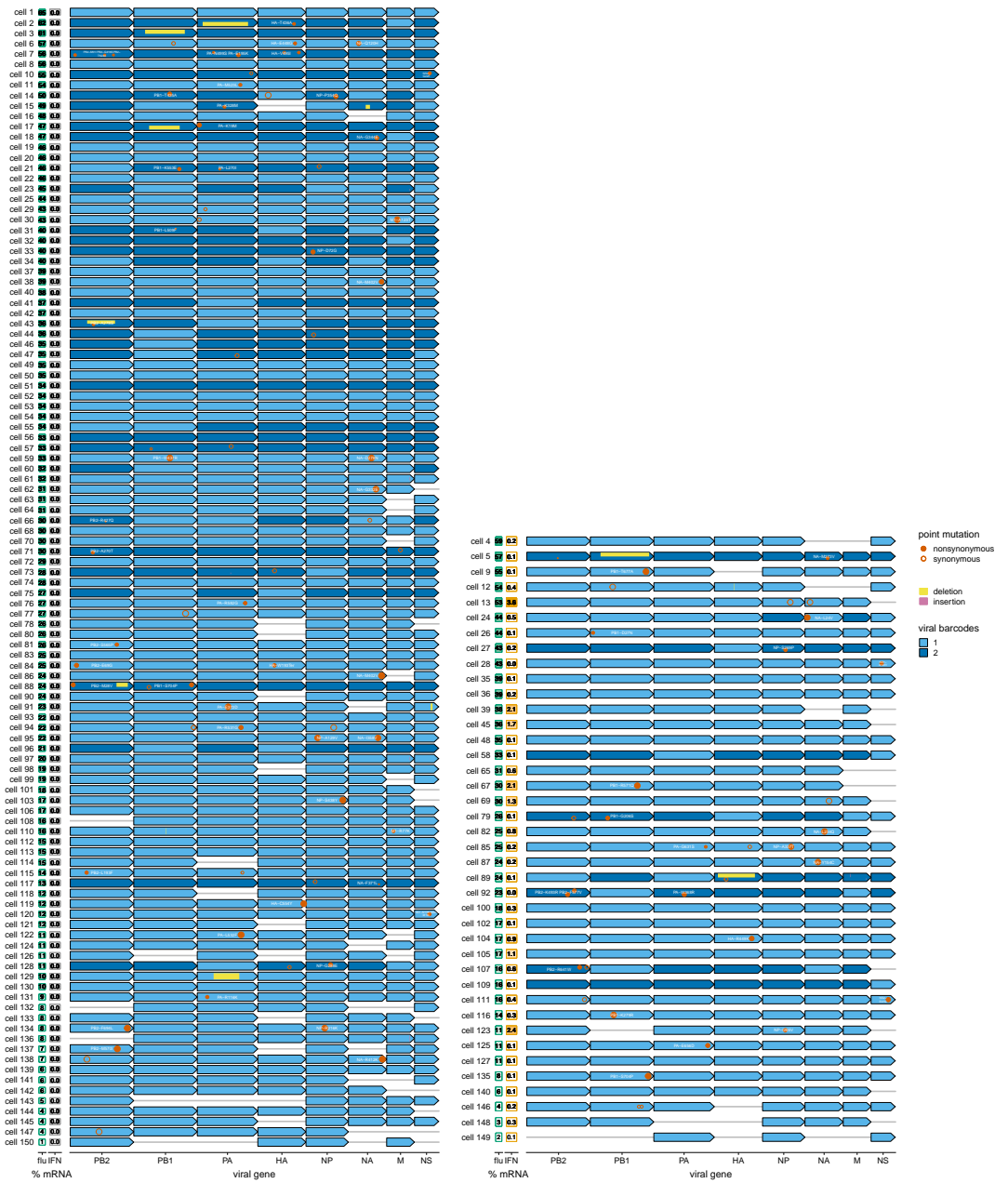


Figure 4-Figure supplement 4. This plot shows the same data as **Figure 4**, but with cells separated into columns based on whether they are IFN- (left column) or IFN+ (right column).

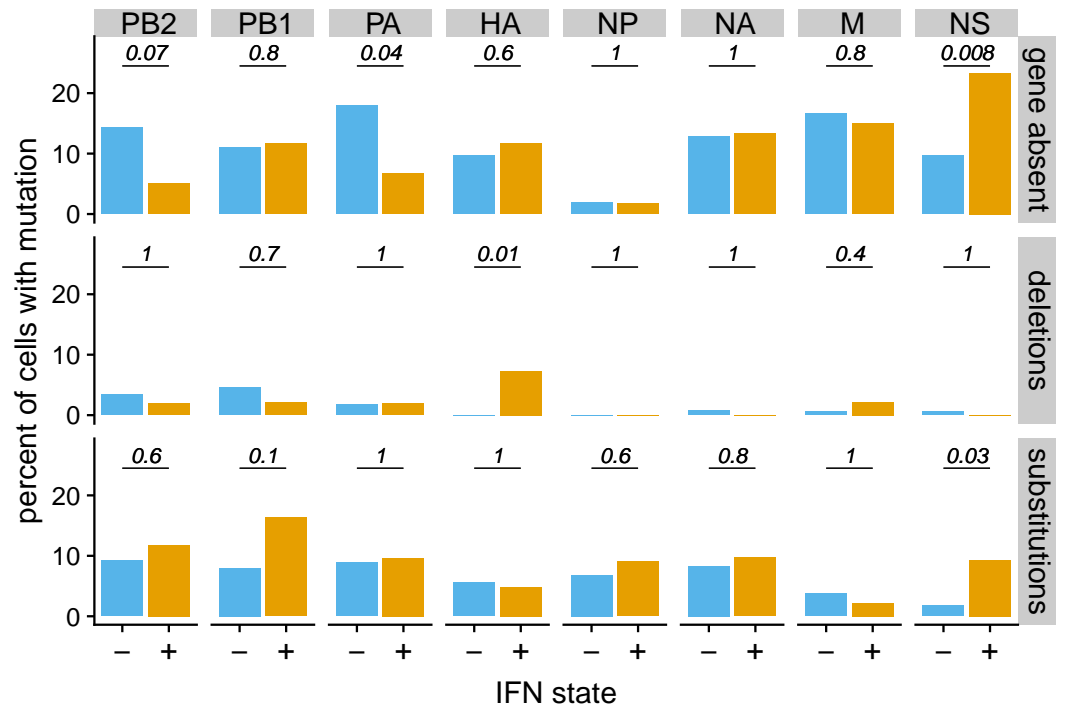


Figure 5-Figure supplement 1. This plot differs from **Figure 5C** in that it also includes data from cells for which some viral genes were not fully sequenced. For incompletely sequenced cells, deletions and substitutions are included in the counts when that particular viral gene is sequenced. The major trends in **Figure 5C** are also true for the larger dataset in this figure. In addition, there is now a modest trend for infected cells that fail to express PB2 and PA *not* to express IFN.

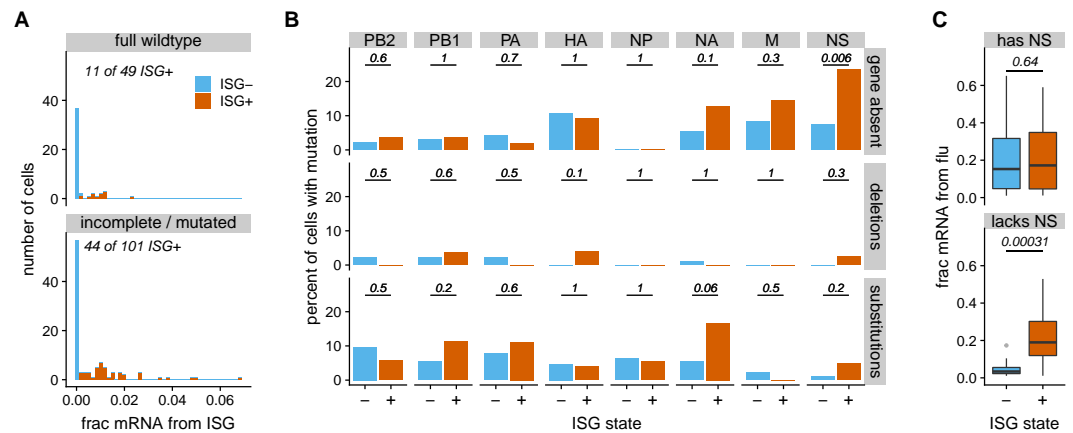


Figure 5-Figure supplement 2. This plot shows the same information as panels **Figure 5B-D** except that it shows the association of viral gene absence / mutations with ISG expression rather than IFN expression. Cells are classified as ISG+ or ISG- as in **Figure 3-Figure Supplement 3**. The major viral features that associate with IFN induction also associate with ISG expression. Specifically, cells that express wild-type copies of all eight viral genes tend to express ISGs less frequently and at lower levels. The absence of NS is strongly associated with higher ISG expression. Viral burden is not associated with ISG expression levels in NS-sufficient infections, but is in NS-deficient infections.

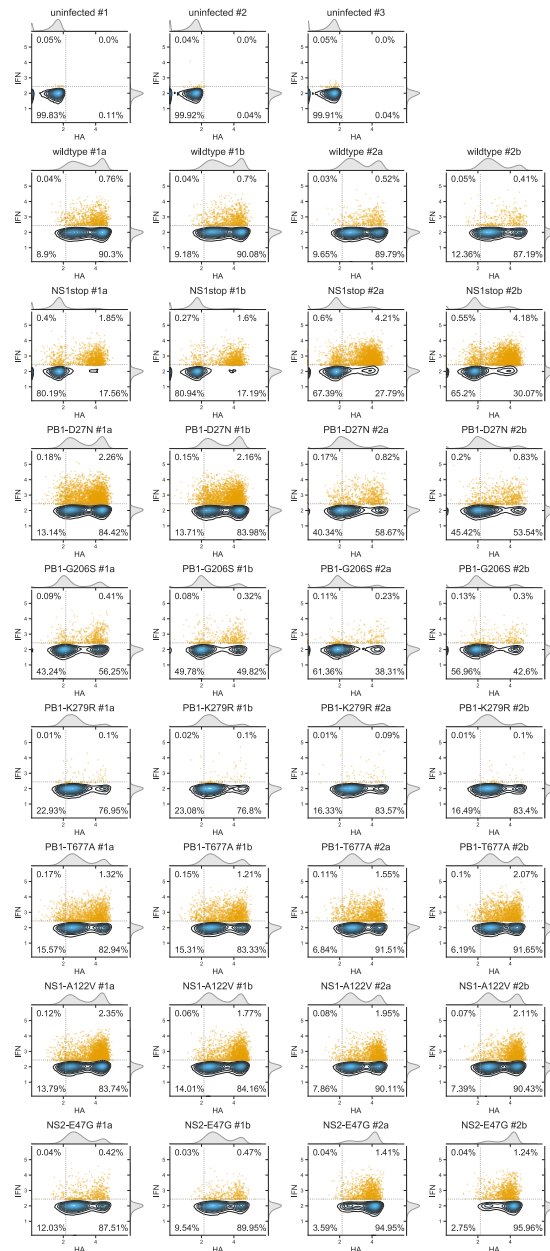


Figure 6-Figure supplement 1. A549 cells with the *IFN1* reporter driving LNGFR Δ C-ZsGreen were not infected (three replicates) or infected with stocks of the indicated viral mutant in quadruplicate. After 13 hours, cells were stained for expression of HA protein and analyzed by FACS for HA and the ZsGreen driven by the *IFN1* reporter. The contour plots show the density of all cells, and IFN+ cells are also indicated by orange dots. Cells were classified as HA+ or IFN+ based on gates set to put 0.05% of the uninfected cells in these populations. For all influenza-infected cells, the percentage IFN+ was calculated only among the HA+ cells (since these are the ones that are infected). For the uninfected cells, the percentage IFN+ was calculated among all cells, since uninfected cells do not express HA. For each viral mutant, two independently generated stocks were each assayed in duplicate (i.e., #1a and #1b are replicates of one viral stock, and #2a and #2b are replicates of the other # viral stock). The infections with replicate #1 of the wild-type virus were performed at an MOI of 0.1 as determined by TCID50, and all other viruses were infected at an equivalent particle number as determined by HI assay. The HA staining indicates that the number of transcriptionally active viral units per cell was similar across most mutants, and calculating percentage IFN+ only among HA+ cells largely corrects for modest variation in titer across mutants.

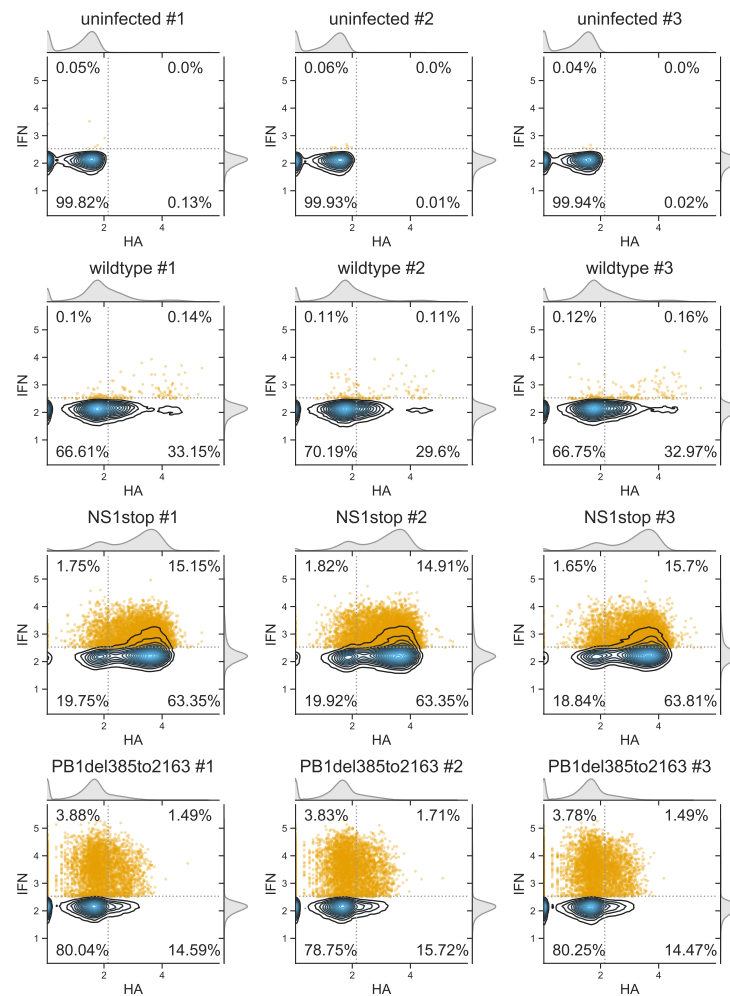


Figure 6-Figure supplement 2. This figure is similar to *Figure 6-Figure Supplement 1* except that it shows the flow cytometry data for **Figure 6B**. Each infection was performed in triplicate. A complicating factor for these data is that the virus with the deletion in PB1 (PB1del385to2163) cannot perform secondary transcription because it does not express PB1 protein, and so cannot be effectively normalized by HA expression since it expresses lower levels of HA due to the lack of secondary transcription. Therefore, for the data in this figure all cells were infected at an equivalent MOI of 0.3 as determined by TCID50 on MDCK-SIAT1 cells for the wild-type and NS1stop viruses, and on MDCK-SIAT1 cells expressing PB1 (*Bloom et al., 2010*) for the PB1del385to2163 virus. Finally, the approach in *Figure 6-Figure Supplement 3* was used to show that equivalent TCID50s, all viral variants had similar amounts of transcriptionally active virus in the absence of secondary transcription. All this normalization suggests that all infections were performed at a similar dose of particles active for primary transcription. Therefore, the percent IFN+ was calculated from the flow data in this figure for *all* cells (HA+ and HA-) since that is a more fair comparison for the PB1del385to2163 virus.

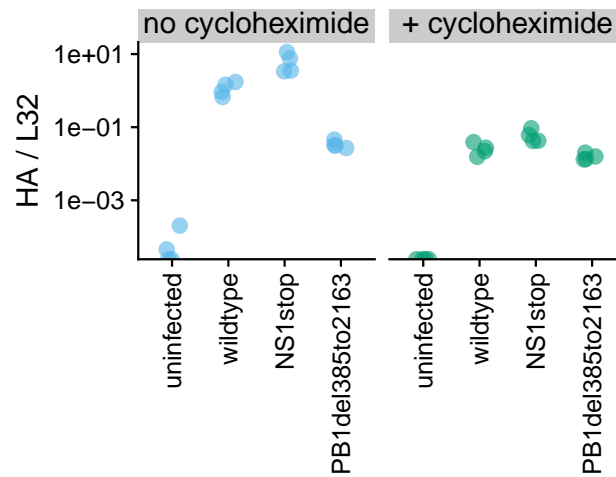


Figure 6–Figure supplement 3. Validation that the infections in **Figure 6B** and **Figure 6–Figure Supplement 2** were performed at similar doses of virions capable of initiating primary transcription. In this experiment, A549 cells were infected at MOI of 0.4 (based on TCID₅₀ as described in **Figure 6–Figure Supplement 2**), and then after 8 hours mRNA was harvested for qPCR on oligo-dT primed reverse transcription products. The y-axis shows the ratio of viral HA mRNA to the housekeeping gene L32. These infections were performed in the presence of absence of 50 μ g/ml cycloheximide, which blocks protein synthesis and hence secondary transcription by newly synthesized viral proteins (*Killip et al., 2014*). In the absence of cycloheximide, the viruses with deletions in PB1 produced less viral mRNA presumably because they could not produce PB1 protein for secondary transcription. But in the presence of cycloheximide, all viruses produced similar amounts of viral mRNA, indicating that the dose of particles active for primary transcription is roughly equivalent across variants. Each measurement was performed in quadruplicate.